RSC Advances

PAPER

View Article Online
View Journal | View Issue

Cite this: *RSC Adv.*, 2026, **16**, 4959

Use of Swiss chard stems and green pea peel extracts as anticorrosive agents for aluminum in 1 M HCl

H. S. Gadow, *[a] N. M. Abd El-Monem[b] and R. M. El-Settawy[a]

Sustainable plant-based biomass has emerged as a significant resource for corrosion mitigation in metallic alloys. This study evaluated the efficiency of Swiss chard stems (SCS) and green pea peel (GPP) extracts in a 1 M HCl medium as low-cost and low-toxicity inhibitors for inhibiting aluminum corrosion. The inhibition performance of the inhibitors was assessed through a combination of techniques, including weight loss (WL) analysis, surface characterization of the metal samples *via* X-ray photoelectron spectroscopy (XPS) as well as atomic force microscopy (AFM), and electrochemical methods, including electrochemical impedance spectroscopy (EIS) as well as potentiodynamic polarization (PDP). WL indicated that the inhibition efficiency (% I.E.) increased in response to an increase in SCS and GPP extract concentrations, reaching up to 91.5% and 83.1%, respectively, at 250 ppm and 55 °C. Potentiodynamic polarization results confirmed that SCS and GPP extracts function as mixed-type inhibitors. Temperature-dependent studies allowed for the determination of thermodynamic activation parameters, while adsorption behavior was found to conform to the Langmuir isotherm more than the Henry isotherm. XPS along with AFM indicated that an inhibitory layer had formed over the surface of aluminum. Additionally, quantum chemical parameters facilitated a deeper insight into the mechanism of the inhibition. The analysis of the adsorption configuration of SCS and GPP extract molecules on the surface of aluminum specimens was conducted by molecular dynamics simulations. Finally, a comparative economics study was discussed.

Received 8th December 2025
Accepted 14th January 2026

DOI: 10.1039/d5ra09501h

rsc.li/rsc-advances

1. Introduction

Corrosion is an undesirable natural phenomenon that occurs in the case of metal exposure to an environment like water or air, which causes deterioration of metals. Corrosion negatively affects the desired properties of the metal, so corrosion protection is required. The fight against corrosion can be achieved by different methods such as design, material selection, use of protective coatings, cathodic protection, anodic protection, and addition of inhibitors. Environmental concerns have led to acute activity in the development of green inhibitors.

A corrosion inhibitor is supposed to have a zero or quite low level of toxicity to marine life, to be biodegradable, and to not be prone to bioaccumulation. The acceptable time duration over which the chosen inhibitor persists in nature is also the permissible level; 60% have to degrade once 28 days have passed.[1] Inhibitors should be nontoxic, as the toxicity is expressed as LC_{50} and EC_{50}. LC_{50} is defined as LC_{50} (median lethal concentration): the concentration of the inhibitor in the surrounding medium (air or water) that causes death in 50% of the test population after a specified exposure time, while EC_{50} denotes (median effective concentration): the concentration of the inhibitor that induces a defined biological response in 50% of the test population. Various heteroatom-containing inhibitors that contain S, O, P, N, and heavy metals have been proven to have strong inhibiting properties against corrosion as they latch on to the metallic surface and offer protection. The biggest issue has been how to get rid of them safely after use because of their unfavorable impact on the environment. These risks have opened the way for researchers to investigate unfamiliar, inexpensive, environmental corrosion inhibitors.

Corrosion inhibition is achieved when inhibitors adsorb to the surface of the metal, generating a film that serves like a protection to prevent the surface of the metal becoming exposed to the surrounding medium. Corrosion inhibitors derived from plant-based biomass have been found as a promising alternative owing to their availability, lower cost, easy preparation, and environmental friendliness. The inhibitive properties of green inhibitors are related to the existence of components like tannins, alkaloids, and flavonoids. These inhibitors, called green corrosion inhibitors, consist mostly of extracts of non-edible plant portions like leaves, stems, seeds, peels, *etc.* Plant part extracts are frequently utilized in different research studies to lessen the corrosive attack and the destructive tendency of acidic solutions on Al metal surfaces.[2–8]

[a]*Chemical Engineering Department, Higher Institute of Engineering and Technology, New Damietta, Egypt. E-mail: hsgado73@gmail.com*
[b]*Chemical Engineering Department, Faculty of Engineering, Cairo University, Cairo, Egypt*

Aluminum is extensively used in the transport sector, construction, packaging and chemical process engineering where the surface preparation processes such as pickling in acidic media are required to remove the oxides and contaminants before anodizing, coating, welding or bonding occur. The processes of pickling and acid-cleaning of aluminum are frequently performed using hydrochloric acid but the chemical or electrochemical conditions that are effective in dissolving the native Al_2O_3 layer are capable of dissolving base metal, reducing the thickness and pitting formation and degradation of mechanical integrity. By that it is implied that proper corrosion inhibitors must be introduced in the HCl pickling bath to prevent the dissolution of the aluminum but not the oxide layer which must be retained to allow safer operation of the process, increased value of the surfaces, longer life of the equipment and minimum environmental and economic losses of over-pickling and wastage of the metals.[9,10]

The corrosion inhibition action of 99.85% pure aluminum has recently been documented using *Ocimum basilicum* L. oil in 0.5 M HCl.[11] Raghavendra *et al.*[12] also studied the corrosion inhibition action of aluminum, in which tender arecanut seed (TAS) extract was used to block aluminum corrosion of type Al-63400 in 0.5 M HCl. Extracts from the peel of sweet orange,[13] the leaf of *Azadirachta indica*,[14] the leaf of *Justicia Secunda*,[15] and the seed of *Cuminum Cyminum*[16] have also been utilized.

From the previous discussion, it is clear that green extracts have a good anticorrosive effect on prone to corrosion materials. Among these metals, aluminum as well as its alloys have been the point of discussion in multiple publications owing to their significance. Aluminum and its alloys have a wide application in the automotive, aviation, and marine sectors owing to the remarkable resistance to corrosion and their extrusion and rolling capabilities. Aluminum is employed in several industrial applications, including pickling, cleaning, and other preparatory stages that are carried out in acidified solutions.[17] Aluminum is pickled in HCl acid solutions due to its chemical or electrochemical etching.[18] The addition of the suitable corrosion inhibitor is important and aimed at reducing the rate of aluminum deterioration or dissolution, which causes thickness reduction in such an aqueous medium.

This study seeks to explore the inhibition action against corrosion of pure aluminum in 1 molar hydrochloric acid as the corrosive medium by using green inhibitors employing both empirical measurements and theoretical analyses. Also, to give an adequate solution to the immense quantity of waste that is generated from food industries, which causes severe pollution issues and disposal problems in addition to the loss of profitable biomass and nutrients. The inhibitors chosen were extracts from green pea peel and Swiss chard stems in methanol. Peas (*Pisum sativum* L.) are affordable, easy to cultivate, high in protein, and abundant worldwide. The pea pods possess a significant amount of flavonoids such as catechin, epicatechin, and apigenin, as well as polyphenols, including phenolic acids such as quinic acid.[19] Swiss chard (*Beta vulgaris* subsp. cicla), which belongs to the *Amaranthaceae* family, is a leafy vegetable grown worldwide for its nutritional value, especially its mineral content. The leaves and stems of Swiss chard have a broad variety of flavonoids and phenolic acids like syringic acid and kaempferol.[20] *Via* performing the weight loss method, we were able to assess the inhibition effectiveness of the inhibitors. The adsorption mechanism associated with the inhibitors as well as the surface coverage were evaluated through equilibrium investigations. Thermodynamics studies were investigated to verify the viability of the process. The electrochemical mechanism of corrosion was conducted by the electrochemical analyses. Both practical surface examination and theoretical studies (quantum chemical calculations in addition to molecular dynamics simulation) were conducted.

2. Materials

2.1. Preparations of metal

Aluminum samples (pure aluminum), the measurements of the sample were 20 mm × 20 mm × 3.5 mm, were gradually polished with 320, 800, and 1200 degrees of sandpaper for use in chemical tests. The degree of polishing was increased for use in surface analysis until 3000 degrees of sandpaper. Then, they were washed using distilled water and then dried according to standard tests. For electrochemical corrosion tests, the working rod was prepared in 1 cm × 1 cm dimensions of Al metal, then welded with copper wire. Finally, it is enclosed in a glass rod attached to the Al specimen by using epoxy and left for 12 hours to ensure good adhesion. The sample used was sanded with varying degrees of sandpaper (320–1200) until it looked shiny, and then the sheet was washed with distilled water.

2.2. Solutions

In this study, the corrosive media used was hydrochloric acid (1 M) derived from pure HCl 30–34% purchased from El Nasr Pharmaceutical Chemicals Co., Egypt. The concentration of HCl was determined by neutralizing with 0.5 M sodium carbonate, and dilution was employed to obtain the desired concentration. The concentration of the inhibitors was extended from 100 ppm to 250 ppm, and the volume used for the experimental work was 100 ml.

2.3. Preparation of plant extracts

Swiss chard (*Beta vulgaris* subspecies cycla) white stems and green pea (*Pisum sativum* L.) peel extracts were the investigated inhibitors prepared as follows: after the assembly of the stems and empty peels, they were rinsed with distilled water. The prewashed stems and peels are dried separately at 35–40 °C in an oven until reaching constant weight and then milled finely to powder. This powder of the two plant materials was extracted separately using pure methanol purchased from El Nasr Pharmaceutical Chemicals Co. for 14 days and then filtered. The filtrate was evaporated at 40 °C until total vaporization of the alcohol. These extracts, after reaching a dark greenish sticky consistency, were ready for making solutions. Tables B1 and B2 (SI), located in supplementary materials, illustrate the important components of Swiss chard stems (SCS) and green pea peels (GPP) extracts, respectively.[21,22]

3. Methods

3.1. Weight loss measurements

Investigations were carried out in both the presence and absence of several doses from both inhibitors in 1 M HCl for three hours. Weight loss readings were conducted at diverse temperatures starting at 25 to 55 °C. The Al samples, after polishing, were rinsed using distilled water, dehydrated, weighed, and introduced into 100 ml of acidic solution (1 M HCl) in a hanging position, whether the inhibitor is present or not. The tested concentrations from both extracts are 100, 150, 200, and 250 ppm. The measurements of weight-loss were conducted up to 180 min and 90 min was considered a typical intermediate immersion period which gives clear differentiation between inhibited and uninhibited specimens and also falls within the practical range of industrial pickling/cleaning exposure duration of aluminum in acidic environments.[23,24]

Every 30 minutes, Al samples were withdrawn from solutions, subjected to a distilled water rinse, their water was dried up, and they were weighed precisely using a sensitive balance. The inhibition efficiencies (% I.E.) and corrosion rates (C.R.) are determined based on the following equations:[25]

$$\text{C.R.} = [\Delta W/At] \quad (1)$$

$$\%\ \text{I.E.} = [(\text{C.R.}_{(\text{free})} - \text{C.R.}_{(\text{inh})})/\text{C.R.}_{(\text{free})}] \times 100\% = \theta \times 100\% \quad (2)$$

where ΔW, A, t, C.R.$_{(\text{free})}$, and C.R.$_{(\text{inh})}$ indicate average weight loss of Al coupon (mg), surface area of specimen (cm^2), period of contact of Al with acid solution (immersion time in min), corrosion rate for inhibitor-free system (blank), and corrosion rate for extract-inhibited systems, respectively.

3.2. Electrochemical analysis

Electrochemical experiments include three electrodes: aluminum as the working electrode, which has a 1 cm^2 exposed surface area; a platinum sheet was employed as the counter (second) electrode; and a saturated calomel electrode (SCE) was employed as the third (reference) electrode. Electrochemical analyses were performed at 25 °C for 1 M HCl solutions, whether the different doses from the inhibitors were present or not.

3.2.1. Potentiodynamic polarization (PDP) investigation. Potentiodynamic cathodic and anodic polarization was performed at 25 °C in a non-stirred 1 M HCl solution, whether the different doses from the inhibitors were present or not. Prior to electrochemical tests, the stability condition is achieved *via* immersion of the working electrode in the 1 M HCl blank solution free of inhibitors as well as in the inhibited solutions for sufficient time (20 minutes) to reach the steady open circuit potential. The PDP profiles were recorded between −900 and −200 mV *versus* SCE at a scan rate of 1 mV s^{-1} with the use of a Potentiostat/Galvanostat (Gamry PCI 300/4) with DC 105 software to perform calculations, operated *via* a computer that also recorded and stored the data. The corrosion current density (i_{corr}) was estimated through the extrapolation of cathodic and anodic Tafel lines until the intersection with the corrosion potential (E_{corr}). The following formula is implemented to determine the inhibition efficiency (% I.E.) and the surface coverage (θ) values;[26]

$$\%\ \text{I.E.} = [(i_{\text{corr(free)}} - i_{\text{corr(inh)}})/i_{\text{corr(free)}}] \times 100\% = \theta \times 100\% \quad (3)$$

The corrosion current densities, whether the inhibitor is present or not, are expressed as $i_{\text{corr(inh)}}$ and $i_{\text{corr(free)}}$, respectively.

3.2.2. Electrochemical impedance spectroscopy (EIS) measurements. After the electrode was immersed in the working solution for sufficient time, the EIS measurements were documented at open circuit potential (OCP). Using AC signals, EIS measurements were performed in the frequency range of 50 kHz to 0.1 Hz with an amplitude of 5 mV peak to peak by using a Potentiostat/Galvanostat (Gamry PCI 300/4) and a personal computer with EIS 300 software for calculations. Using the resistance, the degree of inhibition is calculated following the relation:[27]

$$\%\ \text{I.E.} = \theta \times 100\% = [(R_{\text{ct}} - R_{\text{ct}}^0)/R_{\text{ct}}] \times 100\% \quad (4)$$

R_{ct} is the charge transfer impedance for the SCS and GPP extracts-inhibited systems, and R_{ct}^0 is that of inhibitor-free systems.

3.3. Surface examinations

Aluminum sheets, the measurements of the sample were 10 mm × 10 mm × 0.5 mm, were employed. Sandpaper was used to polish the Al sheets in several degrees (1000, 1200, 2000 and 3000). The sheets were thoroughly washed using distilled water and gently dried.

3.3.1. Atomic force microscope (AFM) analysis. AFM analysis was conducted to study the surface morphology of the Al specimens. Three assessments were undertaken: the blank solution (1 molar HCl) was used for immersing a polished aluminum sheet, and in the other two assessments, the polished Al sheets were immersed in inhibited solutions containing 1 M HCl in addition to the maximum dose of both extracts (250 ppm) for 6 hours at 303 K. Atomic Force Microscopy scanning was undertaken using a Bruker Dimension Icon scanning probe microscope (Bruker Corporation, Santa Barbara, CA, USA) operated in tapping mode under ambient conditions (temperature 22 ± 2 °C, relative humidity 40 ± 5%). Scan rates were adjusted between 0.5 and 1 Hz depending on the scan size, with image resolution set to 512 × 512 pixels. Multiple areas were scanned on each sample to ensure representative characterization of the surface features, with scan sizes ranging from 1 × 1 μm^2 to 10 × 10 μm^2. Prior to scanning, high-purity nitrogen gas was used to gently clean all samples, removing any loosely adhered contaminants from the surface. The instrument was calibrated using a standard calibration grid before measurements, and the piezoelectric scanner was allowed to equilibrate for at least 30 minutes prior to imaging to minimize thermal drift. Image processing and analysis were conducted using NanoScope Analysis software (version 2.0, Bruker) and included plane fitting, flattening (0th or 1st order),

and statistical calculations of surface roughness parameters, comprising average roughness (S_a), root-mean-square roughness (S_q), and the maximum peak-to-valley height (P–V). Three-dimensional reconstructions were generated to visualize the topographical features, and section analyses were performed to determine the heights and lateral dimensions of specific surface features.

3.3.2. X-ray photoelectron spectroscopy examination (XPS). The morphology of the surface of aluminum sheets was examined after submerging the polished sheets in solutions that contained 1 M HCl along with the maximum dosage of both extracts (250 ppm) for 6 hours at 303 K. XPS measurements were conducted using a Kratos Axis Ultra DLD spectrometer (Kratos Analytical Ltd, Manchester, UK) equipped with a monochromatic Al Kα X-ray source ($h\nu$ = 1486.6 eV) operating at 150 W (15 kV × 10 mA). The analysis was performed under ultra-high vacuum conditions with a base pressure of approximately 1×10^{-9} torr. Data processing and peak fitting were performed using CasaXPS software (version 2.3.24, Casa Software Ltd, UK). A Shirley-type background was subtracted, and peak fitting was carried out using mixed Gaussian–Lorentzian (70 : 30) functions. Atomic concentrations were calculated from peak areas normalized by Scofield sensitivity factors and the transmission function of the analyzer.

The duration of immersion was chosen to be 6 h at 303 K in order to deepen and stabilize the surface roughness and adsorbed inhibitor films to give more definition of morphological and chemical distinctions between uninhibited and inhibited aluminum than shorter immersion times.

3.4. Theoretical studies

3.4.1. Quantum chemical calculations. In Material Studio 7.0, the DMol^3 module was utilized to investigate molecules. The GGA, the popular gradient approach, was added to a combination of the chosen basis set which was DNP (double-digit polarization) with BOP (Becke One interchangeable relationship functions), and the COSMO was used to manage the solvent effects Within this DMol^3 tool. Criteria including the highest occupied molecular orbital energies (E_{HOMO}) along with the lowest unoccupied molecular orbital energies (E_{LUMO}), electronegativity, an energy gap calculated between LUMO and HOMO, softness, chemical potentials, global hardness, and the number of electrons transferred were determined; the following equations define each of them:[28]

$$I, \text{(ionization potential)} = -E_{HOMO} \quad (5)$$

$$A, \text{(electron affinity)} = -E_{LUMO} \quad (6)$$

$$\text{Pi, (chemical potential)} = -\chi \quad (7)$$

$$\text{Pi} = (E_{LUMO} + E_{HOMO})/2 \quad (8)$$

$$\eta, \text{(global hardness)} = \Delta E/2 = (E_{LUMO} - E_{HOMO})/2 \quad (9)$$

$$\sigma, \text{(softness)} = 1/\eta \quad (10)$$

$$\omega, \text{(electrophilicity index)} = \text{Pi}^2/2\eta \quad (11)$$

$$\varepsilon, \text{(nucleophilicity index)} = 1/\omega \quad (12)$$

$$\Delta E \text{ back donation} = -\eta/4 \quad (13)$$

$$\omega^+, \text{(electro-accepting power)} = (I + 3A)^2/16(I - A) \quad (14)$$

$$\omega^-, \text{(electro-donating power)} = (3I + A)^2/16(I - A) \quad (15)$$

$$\Delta N, \text{(the proportion of transported electrons)} = (\chi_{Al} - \chi_{inh})/2(\eta_{inh} + \eta_{Al}) \quad (16)$$

The symbols χ_{inh} and χ_{Al}, respectively, indicate the absolute electronegativity values for the inhibitor and aluminum metal. The electronegativity and hardness for aluminum are 3.23 eV mol^{-1} and 0 eV mol^{-1}, respectively.[23]

3.4.2. Molecular dynamics simulation. Software, Material Studio 7.0 from BIOVIA Accelrys, was used to conduct MD simulation studies. The adsorption locator simulates particle adsorption of pea peel and Swiss chard stem extracts onto an aluminum surface. The Al (1 1 1) plane was extended to a (10 × 10) supercell to offer a broad surface area to investigate its interfacial relation with the inhibitors. Subsequently, above the Al (1 1 1) plane, a vacuum slab whose thickness is 32 Å was constructed. Pea peel and Swiss chard stem extracts' molecular energy optimization was performed using the Forcite classical simulation engine. The corrosion system, comprised of the aluminum surface along with molecules of extracts in water containing HCl acid, was constructed in the aquatic medium through a layer builder. The COMPASS simulation study with a force field was adopted to model the potential for both extract particles to adsorb on the Al surface (111).

3.5. Response surface methodology (RSM)

Response Surface Methodology was adopted with temperatures of −1, 0, +1 coded as A, B, C −1 M HCl to optimize the corrosion inhibition parameters of aluminum using Swiss chard stems (SCS) and green pea peel (GPP) extracts, the Design-Expert software (version 13, Stat-Ease Inc., Minneapolis, MN, USA) utilized a Box–Behnken Design (BBD) with 20 independent runs (five center points to determine reproducibility), with measured responses included inhibition efficiency and corrosion rate. A second-order polynomial model was employed to fit the data, $Y = \beta_0 + \beta_1 A + \beta_2 B + \beta_3 C + \beta_{11} A^2 + \beta_{22} B^2 + \beta_{33} C^2 + \beta_{12} AB + \beta_{13} AC + \beta_{23} BC + \varepsilon$, and model significance was measured by ANOVA (p = 0.05 terms significant) and diagnostics included normal probability plots of studentized residual, predicted and actual plots and lack of fit tests to ensure the adequacy of the model without higher-order terms; this model is consistent with recent studies.[29–31]

4. Results and discussion

This work primarily seeks to protect the aluminum metal from corrosion through utilizing pea peel and Swiss chard stem methanol extracts. This purpose was achieved by examining the

effectiveness of these extracts towards inhibiting metal corrosion. Below are the results of the tests that were performed on the metal and their indications.

4.1. Weight-loss (WL) tests

Green pea pod (GPP) and Swiss chard stem (SCS) extracts were utilized in WL tests to inhibit aluminum corrosion. The inhibition was confirmed as corrosion rates were calculated. WL tests of Al in one molar HCl solution, whether the inhibitor is present or not and with concentrations ranging from 100 to 250 ppm, were performed. These tests were conducted at different time periods and various temperatures (298–328 K). Tables 1 and 2 illustrate the relationship between the effectiveness of inhibition and the temperature of the medium in the existence and non-existence of specific doses from Swiss chard stems and green pea peel extracts after 90 minutes of immersion, respectively.

The corrosion rate is reduced as the inhibitor molecules are introduced. When 250 ppm from SCS and GPP extracts were present, the inhibition efficiency was increased to 91.5% and 83.1%, respectively, after 90 minutes of immersion time and a temperature of 55 °C. The presence of a molecular film from the extract over the Al surface is responsible for the elevation in the inhibition value upon an increase in the concentration level of both extracts. The formed layer functions as a protective barrier to prevent the corrosive environment (HCl) from direct contact with the metal surface (Al). Additionally, Fig. 1 and 2 illustrate how temperature affects the extent to which aluminum is inhibited from corroding in hydrochloric acid and the corrosion rate obtained after an immersion period of 90 minutes. The maximum inhibition is obtained at 55 °C as the inhibition rises with the temperature rise. This outcome may be clarified by the cathodic process behavior of hydrogen liberation in acidic media. As the temperature rises, the hydrogen liberation increases, which accelerates the rate of the cathodic reaction. On the contrary, a rise in temperature boosts the formation of chemisorbed inhibitor layers on the Al surface. Once the latter effect gains dominance, the outcome is a predominant inhibitory effect. Other authors discovered similar outcomes.[32–34]

The weight loss over time at various temperatures is illustrated in Fig. A1 and A2 (SI) for SCS and GPP extracts, respectively. The plots demonstrate two main relationships in the case of Al submerged in 1 M HCl: a marked decline in corrosion rates in response to the addition of both extracts, indicating that the extract suppressed the corrosion, and an increase in corrosion rates with prolonged exposure time for all systems, particularly in the uninhibited medium. The increased efficiencies at 55 °C are realistic high-temperature conditions that apply to industrial cleaning/pickling, and thus they are a harsh but realistic situation.[35,36]

To compare the performance of SCS and GPP, Table 3 will compare the maximum inhibition efficiency of a number of reported plant-based inhibitors of aluminum in the hydrochloric acid media at similar conditions.

According to this literature comparison, a large number of green inhibitors of aluminum in 1 M (or 0.5 M) HCl often achieve maximum efficiencies in the 80–90 percent range at room (or moderately elevated) temperature, and often at higher doses than those used here. Some examples are *Cicer arietinum*, coriander seeds, *Ajuga orientalis*, *Trigonella foenum-graecum* oil, lavender oil, *Juglans regia*, *Ocimum basilicum* oil, and *Phoenix dactylifera* leaves with the resultant inhibition efficiencies comparable to the highest values reported to date of SCS and GPP in the same aggressive environments. This reflects the fact that SCS and GPP have performed on par with other plant-based systems already deemed promising in the role of aluminum inhibitor with acidic media, which are regarded as

Table 1 Data of WL of aluminum in 1 M HCl solution for several doses of Swiss chard stem (SCS) extract after 90 minutes of immersion time

Temp. (°C)	Conc. (ppm)	Δw (mg cm^{-2})	C.R. (mg cm^{-2} min)	θ	% IE
25	Blank	0.3086	0.0034		
	100	0.1162	0.0013	0.624	62.4
	150	0.1095	0.0012	0.645	64.5
	200	0.1071	0.0012	0.653	65.3
	250	0.0979	0.0011	0.683	68.3
35	Blank	0.9357	0.0104		
	100	0.2884	0.0032	0.692	69.2
	150	0.1939	0.0022	0.793	79.3
	200	0.1842	0.0020	0.803	80.3
	250	0.1418	0.0016	0.849	84.9
45	Blank	16.1562	0.1795		
	100	4.1672	0.0463	0.742	74.2
	150	3.1850	0.0354	0.803	80.3
	200	2.5000	0.0278	0.845	84.5
	250	1.5417	0.0171	0.905	90.5
55	Blank	63.2460	0.7027		
	100	14.0536	0.1562	0.778	77.8
	150	11.9196	0.1324	0.812	81.2
	200	9.2121	0.1024	0.854	85.4
	250	5.3733	0.0597	0.915	91.5

Table 2 Data of ML of aluminum in 1 M HCl solution for several doses of green pea peel (GPP) extract after 90 minutes of immersion time

Temp. (°C)	Conc. (ppm)	Δw (mg cm^{-2})	C.R. (mg cm^{-2} min)	θ	% IE
25	Blank	0.2778	0.0031		
	100	0.0998	0.0011	0.641	64.1
	150	0.0968	0.0011	0.652	65.2
	200	0.0871	0.0010	0.686	68.6
	250	0.0833	0.0009	0.700	70.0
35	Blank	2.0242	0.0225		
	100	0.7036	0.0078	0.652	65.2
	150	0.6679	0.0074	0.670	67.0
	200	0.6196	0.0069	0.694	69.4
	250	0.5877	0.0065	0.710	71.0
45	Blank	10.9722	0.1219		
	100	3.3418	0.0371	0.695	69.5
	150	2.8086	0.0312	0.744	74.4
	200	2.4760	0.0275	0.774	77.4
	250	1.8710	0.0208	0.830	83.0
55	Blank	50.3711	0.5597		
	100	14.4871	0.1610	0.712	71.2
	150	12.0663	0.1341	0.761	76.1
	200	10.2651	0.1141	0.796	79.6
	250	8.5366	0.0949	0.831	83.1

environmentally friendly. In addition, temperature trends (which tend to drop efficiency with temperature, or not monotonic) are consistent with those found in these studies, which lends the interpretation of mixed physisorption/chemisorption behavior. In general, this comparison proves that the current extracts fall in the same category as successful green inhibitors and competitive inhibition efficiencies as compared to those of previously reported natural products.

4.2. Parameters of activation through thermodynamics

For a deeper insight into the corrosion-inhibiting properties of the inhibitors and the corrosion response to temperature changes, the activation thermodynamic parameters of the corrosion operation have to be evaluated whether the inhibitor is present or not. An Arrhenius equation as well as transition state equation were used to estimate the activation energy (E_a), the enthalpy (ΔH_a), and the entropy of activation (ΔS_a) as follows:[43]

$$\ln \text{C.R.} = -\frac{E_a}{RT} + \ln A \tag{17}$$

$$\ln \frac{\text{C.R.}}{T} = \left[\ln \frac{R}{N_A h} + \frac{\Delta S_a}{R}\right] - \frac{\Delta H_a}{RT} \tag{18}$$

The variables T, R, h, and N_A represent the absolute temperature, the universal gas constant, Planck's constant, and Avogadro's number, respectively. The constant (A) is the Arrhenius pre-exponential factor. As illustrated in Fig. 3, linear regression between (ln C.R.) and $\left(\frac{1}{T}\right)$ was used to determine the activation energy at various inhibitor doses. The kinetic model was able to demonstrate the corrosion of aluminum as indicated by the linear regression coefficient approaching nearly unity. The computed results of the activation energy are provided in Table 4 which are determined from the slope of the plots of (ln C.R.) *versus* $\left(\frac{1}{T}\right)$.

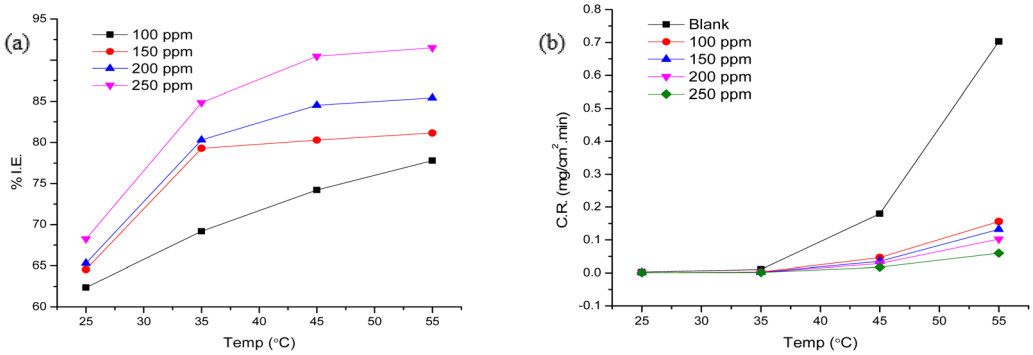

Fig. 1 Aluminum inhibition efficiency (a) and corrosion rate (b) after 90 minutes of immersion in 1 M HCl at various temperatures (25–55 °C), at different Swiss chard extract concentrations (100–250 ppm).

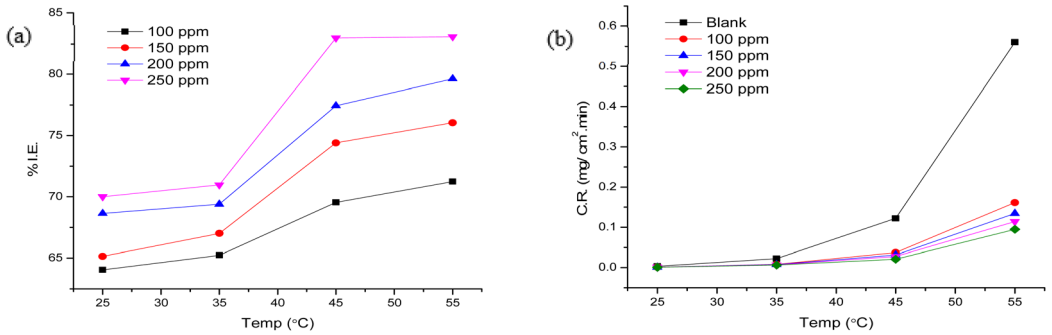

Fig. 2 Aluminum inhibition efficiency (a) and corrosion rate (b) after 90 minutes of immersion in 1 M HCl at various temperatures (25–55 °C), at different pea peel extract concentrations (100–250 ppm).

According to the calculations, E_a decreases when SCS and GPP extracts are present. This is mostly due to differences in the rates of SCS and GPP adsorption and metal dissolution. As the temperature rises, more chemisorption occurs, resulting in a much higher quantity of adsorbed molecules over the surface. This promotes the equilibrium to shift toward more adsorption and less desorption.[44] The process by which the inhibitor molecule donates charge to the Al surface, thereby generating a coordination bond, is known as chemisorption. The mechanism of chemical adsorption of the extracts is supported by the decrease of E_a in inhibited solutions and the aforementioned variation of protective action with temperature. Chemisorption is responsible for a lower activation energy value when the inhibitor is introduced *versus* when it is not, but physical adsorption has the opposite influence.[45] The rise in E_a when the inhibitor is present suggests the physical adhering of the molecules to the surface or that there is a weak chemical interaction between them. Also, 80 kJ mol^{-1} is the threshold value needed for the chemisorption mechanism, which also supports the previous findings.[46,47] This observation suggests that the corrosion process is surface-reaction controlled, owing to the activation energy exceeding 20 kJ mol^{-1} under both inhibited and uninhibited conditions.[48]

The values of the enthalpy and the entropy of activation were evaluated by plotting the graphical representation of $\left(\ln\frac{C.R.}{T}\right)$ against $\left(\frac{1}{T}\right)$ as shown in Fig. 4. A straight line is plotted with a slope of $\left(\frac{-\Delta H_a}{R}\right)$ and an intercept of $\left[\ln\left(\frac{R}{N_A h}\right)+\frac{\Delta S_a}{R}\right]$, enabling extraction of ΔH_a and ΔS_a values, and these values are presented in Table 4. The positive value of ΔH_a indicates the

Table 3 Efficiencies of maximum inhibition of the chosen plant-based green inhibitors with aluminum in media of hydrochloric acid and their comparison with the current research

Plant extract	Corrosive medium	Metal	% I.E.	References
Cicer arietinum extract	1 M HCl	Al (99.99%)	(% I.E. is % 91.1 at 150 ppm, 25 °C) the efficiency decreases with increasing temperature	37
Coriander seeds extract	1 M HCl	Pure Al	(% I.E. is % 82.4 at 0.522 g L^{-1}, 35 °C)	38
Ajuga orientalis L. Extract	1 M HCl	Aluminum foil specimens	(% I.E. is %84 at 300 ppm, 50 °C) efficiency decreases up to 40 °C, then increases up to 50 °C	39
Different extracts of *Trigonellafoenum-graecum* L seeds	1 M HCl	Aluminum	(% I.E. is 84.41% for the extract with ethanol, 86.6% for the extract with dichloromethane and 75.77% for the extract with pentane at 1400 ppm, 25 °C)	4
Lavender essential oil	1 M HCl	Al (99.85%)	(% I.E. is %90.2 at 500 ppm, 25 °C)	40
Juglans regia L. extract	1 M HCl	Al (99.8%)	(% I.E. is %88.8 at 0.14 g L^{-1})	41
Ocimum basilicum L. Oil	0.5 M HCl	Al (99.85%)	(% I.E. is %78.4 at 5.7 g L^{-1}, 30 °C)	11
Phoenix dactylifera L. leaves	0.5 M HCl	Al (99.55%)	(% I.E. is %89.1 at 1000 ppm, 20 °C)	42

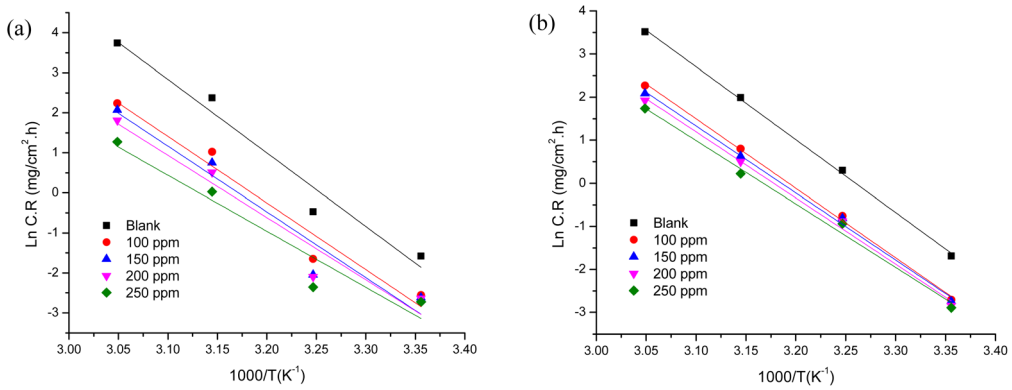

Fig. 3 Arrhenius plots for aluminum in 1 M HCl in the existence and non-existence of specific concentrations from (a) SCS and (b) GPP extracts after 90 minutes of immersion.

heat-absorbing nature of aluminum dissolution in 1 M HCl. Thus, the inclusion of inhibitors decelerates the rate of Al dissolution.[49] Additionally, decreased enthalpy of activation values associated with the existence of SCS and GPP extract molecules reveal the inhibition efficiencies rise as the temperature rises. The higher E_a values compared with ΔH_a imply that the reaction mechanism involves a gaseous-phase reaction, basically the hydrogen liberation reaction, was engaged in the corrosion process, associated with a drop in the overall reaction volume.[50] The activation entropy characterizes the molecular energy redistribution that enables the reaction to take place. The activation entropies were positive, implying that the reaction was feasible and spontaneous and that the activation complex represents association stages. The literature contains similar interpretations.[51,52] As inhibitor concentration rises, positive entropy (ΔS_a) values drop, suggesting less disorder as reactants shift into the activated complex.[53]

4.3. Adsorption isotherm and adsorption parameters

It is essential to understand the behavior of adsorption inhibitors so as to identify their inhibition mechanism, as the primary cause of the corrosion inhibition of organic compounds using the plant extract is their adsorption in the interfacial region separating the metal and solution. Adsorption isotherms are a useful approach for obtaining fundamental information on the extract's interactions with the Al surface. A number of isotherms, including the Frumkin, the kinetic thermodynamic model of El-Awady *et al.*, Henry, Flory-Huggins, Freundlich, Temkin, and the Langmuir adsorption models, were created from weight loss studies at different temperatures. To identify the isotherm that best describes the adsorption process, the degree of surface coverage data obtained from WL tests over the temperature range of 298–328 K was employed. Data on surface coverage against concentration were fitted using a variety of adsorption isotherm models (Fig. 5, 6, SI Fig. A3, and A4). The best-fit isotherm was identified using the correlation coefficient (R^2) after the graphical fitting of the adsorption isotherms mentioned above. Values of the correlation coefficient were illustrated in Tables B3 and B4. The best fit among these models was offered mainly by the Langmuir model rather than the Henry model. Consequently, the Langmuir isotherm was established to serve as the most appropriate explanation describing the adsorption mechanism of SCS and GPP extracts on the Al surface. The following equations are related to the Langmuir and the Henry isotherm models.[54]

$$\text{Henry: } \theta = K \times C \tag{19}$$

$$\text{Langmuir: } \frac{C}{\theta} = \frac{1}{K} + C \tag{20}$$

The equilibrium constant of the adsorption process (K_{ads}) values were evaluated based on the intercepts of the $\left(\frac{C_{inh}}{\theta}\right)$ axes of the Langmuir model and the slope of the Henry isotherm model. An increased K_{ads} value with increased temperature indicates that the inhibitor molecules have

Table 4 Activation parameters for Al corrosion in 1 M HCl in the existence and non-existence of specific concentrations from both plant extracts

	Swiss chard stems extract			Green pea peels extract		
Conc. (ppm)	E_a (kJ mol^{-1})	ΔH_a (kJ mol^{-1})	ΔS_a (J mol^{-1} K)	E_a (kJ mol^{-1})	ΔH_a (kJ mol^{-1})	ΔS_a (J mol^{-1} K)
Blank	152.67	150.07	243.21	140.67	138.07	204.94
100	138.36	135.76	187.01	134.18	131.58	174.79
150	136.60	134.00	179.53	129.48	126.89	158.85
200	129.29	126.69	154.96	127.73	125.13	152.27
250	116.48	113.88	111.14	122.43	119.83	134.13

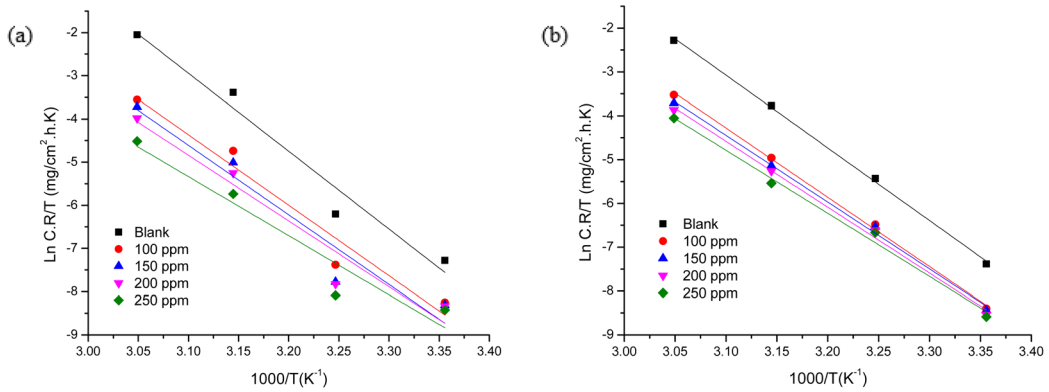

Fig. 4 Transition state plots for aluminum in 1 M HCl in the existence and non-existence of specific concentrations from (a) SCS and (b) GPP extracts after 90 minutes of immersion.

a stronger bond with the metal surface in consequence of the chemical adsorption. The standard free energy of adsorption (ΔG^0_{ads}) is linked to K_{ads} through the next relation as illustrated in Tables 5 and 6.[55]

$$\Delta G^0_{ads} = -RT\ln(55.5\ K_{ads}) = \Delta H^0_{ads} - T\Delta S^0_{ads} \quad (21)$$

where 55.5 mol L^{-1} represents water molecules' concentration. Chemical adsorption happens once the calculated value of the free energy is greater than −40 kJ mol^{-1}. Values below −20 kJ mol^{-1} correspond to physical adsorption, and values between −20 and −40 kJ mol^{-1} imply mixed adsorption.[56] All calculated values of the adsorption free energy according to the Langmuir model observed in the current system indicate a comprehensive adsorption (physicochemical adsorption), but chemisorption is the main process.[57] The negative ΔG^0_{ads} values assure the stability of the molecular film adsorbed on the Al substrate as well as the spontaneous nature of the adsorption mechanism. Values of $\log K_{ads}$ are plotted *versus* $1000/T$ as illustrated in Fig. 7 to provide a greater understanding of the adsorption characteristics from the perspective of enthalpy along with entropy of adsorption. The enthalpy of adsorption ΔH^0_{ads} can be determined with the use of the integrated expression of the Van't Hoff formula as follows:[58]

$$\ln K_{ads} = (-\Delta H^0_{ads}/RT) + (\Delta S^0_{ads}/R) + \ln(1/55.5) \quad (22)$$

The enthalpy (ΔH^0_{ads}) and entropy of adsorption (ΔS^0_{ads}) are computed in Tables 5 and 6. The inhibitor's adsorption process is an endothermic process, as indicated by the positive enthalpy of adsorption values. A ΔH^0_{ads} value below zero indicates a physisorption mechanism, while a value over zero indicates chemical adsorption, as in the current investigation.[59] The positive ΔS^0_{ads} values that are obtained indicate that the surface adsorption of the extract conducted through the desorption of additional water molecules leads to increased disorder.[60] As a result, the adsorption entropy increases. Similar interpretations can be found in previous works.[61]

4.4. Potentiodynamic polarization (PDP) technique

It is a well-documented fact that the behavior of metal's oxide layer mainly determines its corrosion behavior (resistance). From Fig. 8 it is noticeable that no passive film formed during the anodic polarization in an inhibitor-free 1 M HCl solution. It is probable that the coupled effect of acid and chloride leads to pitting conditions, provided the acidic environment is capable of dissolving the naturally formed oxide layer on aluminum. The diffusion of aluminum atoms into the hydrochloric acid solution is facilitated by the reduction in oxide film resistance caused by chlorides replacing oxygen atoms within the oxide

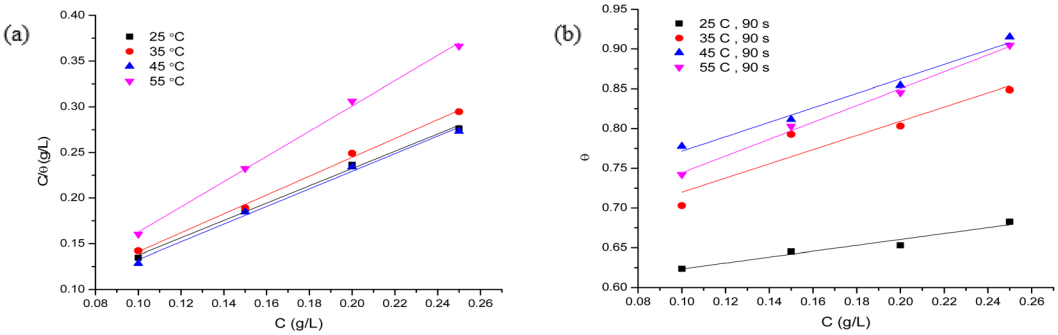

Fig. 5 (a) Langmuir and (b) Henry adsorption isotherm models of 1 M HCl solution and containing various concentrations of SCS extract.

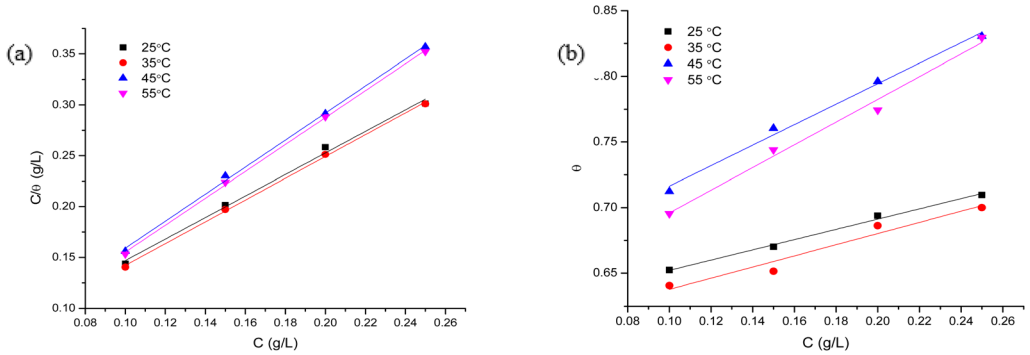

Fig. 6 (a) Langmuir and (b) Henry adsorption isotherm models of 1 M HCl solution and containing various concentrations of GPP extract.

structure. The film dissolves more quickly than it forms, and a strong metal dissolution takes place.[62]

Potentiodynamic anodic and cathodic polarization scanning were performed using varying doses of SCS and GPP extracts in 1 M HCl. Fig. 8 displays anodic and cathodic polarization curves at various doses with and without inhibitors at 25 °C. Tafel plots exhibit identical behavior for both inhibited and uninhibited Tafel lines without any indication of passivation within the potential range under study, indicating that the inhibitor blocked the adsorption-active sites of the aluminum surface without influencing the corrosion mechanism. The incorporation of the inhibitors leads to a slight variation in the anodic Tafel slope (β_a) and cathodic (β_c) Tafel slope. An approximately parallel alignment is observed in the cathodic curves, reflecting a slowdown in the hydrogen evolution reaction and controlled activation; in addition, the reduction mechanism is not affected by increasing concentration.[63] Also, the curves are parallel in the anodic region. Table 7 provides a summary of the values of several electrochemical parameters from Tafel plots.

When inhibitors were added, the corrosion potential values slightly changed. There is no regular or consistent change in corrosion potential upon incorporation of the inhibitor. Additionally, there is no systematic variation in the cathodic and anodic Tafel slopes. This observation suggests that SCS and GPP extracts function as mixed-type inhibitors, encouraging the retardation of the cathodic hydrogen liberation reactions and the anodic metal dissolution. A mixed-type inhibitor was identified if the E_{corr} shift relative to the E_{corr} of the blank solution was less than ± 85 mV, and an anodic or cathodic inhibitor was identified if the E_{corr} displacement values were greater than ± 85 mV.[64] It was revealed that the currents for both the cathodic and anodic reactions are decreasing relative to the blank solution that is not inhibited, demonstrating that a protective deposit of the extracts built up on the Al surface. The inhibition efficiency (I.E.%) increased as a result of the corrosion current decreasing. The rise in I.E.% at greater inhibitor concentrations suggests that the surface adsorption improved upon increasing the inhibitor dosage. This results in more inhibitor molecules being adsorbed over the metal surface, thus leading to a large surface coverage. Weight loss outcomes and Tafel polarization data were in reasonable agreement.

4.5. Electrochemical impedance spectroscopy (EIS)

EIS studies include details on the surface characteristics of the systems under investigation. Information can be deduced from the shape of the impedance diagram. The EIS technique was implemented to evaluate the corrosion efficiency of aluminum metal in inhibited and inhibitor-free 1 M HCl solutions at 25 °C. The equivalent circuit in Fig. 9, consists of a parallel setup of a constant phase element and charge-transfer resistance, aligned in serial configuration with the solution resistance, to analyze every step of the system's electrical behavior.[65]

Table 5 Langmuir and Henry isotherms for the adsorption of Swiss chard extract on the Al surface at various temperatures

Temp. (°C)	R^2	log K	$-\Delta G_{ads}$ (kJ mol^{-1})	ΔH_{ads} (kJ mol^{-1})	ΔS_{ads} (J mol^{-1} K^{-1})
Langmuir isotherm					
25	0.99457	4.371	24.942	13.860	130.210
35	0.99585	4.422	26.078		129.670
45	0.99055	4.443	27.052		128.656
55	0.99688	4.614	28.977		130.600
Henry isotherm					
25	0.93101	2.567	14.649	26.210	137.112
35	0.84527	2.951	17.405		141.606
45	0.97353	2.959	18.014		139.070
55	0.99331	3.025	18.999		137.833

Table 6 Langmuir and Henry isotherms for the adsorption of green pea extract on the Al surface at various temperatures

Temp. (°C)	R^2	log K	$-\Delta G_{ads}$ (kJ mol^{-1})	ΔH_{ads} (kJ mol^{-1})	ΔS_{ads} (J mol^{-1} K^{-1})
Langmuir isotherm					
25	0.99342	4.388	25.035	16.469	139.277
35	0.99869	4.457	26.285		138.814
45	0.99776	4.581	27.894		139.507
55	0.99915	4.640	29.138		139.046
Henry isotherm					
25	0.99144	2.592	14.792	24.236	130.965
35	0.93452	2.630	15.508		129.039
45	0.98961	2.892	17.610		131.593
55	0.98357	2.937	18.445		130.125

In the equivalent circuit structure, the constant phase element (CPE) was used in place of the ideal double-layer capacitance (C_{dl}). CPE provides a variety of heterogeneities that are appropriate for corrosion electrodes, such as grain boundaries, surface contaminants, deficient polishing, and surface roughness.[66] The experimental results demonstrate how well this model fits the data. Through raising the inhibitor doses, the C_{dl} values decrease and the R_{ct} values increase, according to the EIS results in Table 8. The exchange of the water molecules that have been adsorbed over the metal surface with the SCS and GPP extract molecules slows down the metal electrochemical dissolution. This shows that the protective molecules work *via* adsorption at the interfacial region between aluminum and the solution. The decrease in C_{dl} can be brought on by the double electrical layer becoming thicker or the local dielectric constant decreasing.[67] The equation for frequency, which has a major impact on element impedance,[68]

$$Z_{CPE} = Y_0^{-1} (j\omega)^{n-1} \quad (23)$$

The CPE parameter is denoted by the symbol Y_0 in the preceding equation, while the imaginary number and sine wave angular frequency are given by the expressions ω and $j^2 = -1$, respectively. The AC frequency is indicated by f and the symbol ω is the equivalent of $2\pi f$. There are many factors that cause n values to vary from 0 to 1, including surface heterogeneity, dielectric constant, and electrode roughness. The results of our analysis indicate that the metal surface is rather homogenous, but the inhibitor adsorption is not uniform since the n value of 1 molar HCl without inhibitor is slightly high when compared with the inhibited system, and the rate drops as the inhibitor concentration is increased.[69] In order to figure out the double layer amplitude (C_{dl}), the following formula was employed:[70]

$$C_{dl} = Y_0 \omega^{n-1} / \sin[n(\pi/2)] \quad (24)$$

A variety of impedances arise due to the adsorption of the anions and cations, and many obstructions are caused by charges that are traveling across or far away from the aluminum surface. Aluminum-resistant properties in 1 M of HCl, whether the inhibitor is present or not, are represented by the data in Table 8. The semi-circular impedance plot in the present study illustrates that aluminum corrosion is governed by the charge migration process. As shown in the Nyquist diagram (Fig. 10), the semicircle diameter increases as the concentration of the tested extracts rises. The charge transfer resistance (R_{ct}) data could be determined *via* the equation given below.[71]

$$R_{ct} = Z' \text{ (at low } f) - Z' \text{ (at high } f) \quad (25)$$

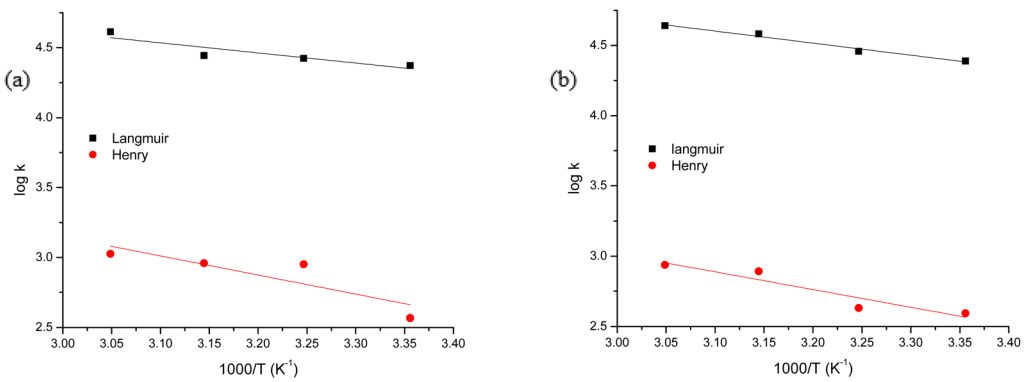

Fig. 7 Van't Hoff equation representation for (a) SCS and (b) GPP extracts (relation among the adsorption equilibrium constant and absolute temperature).

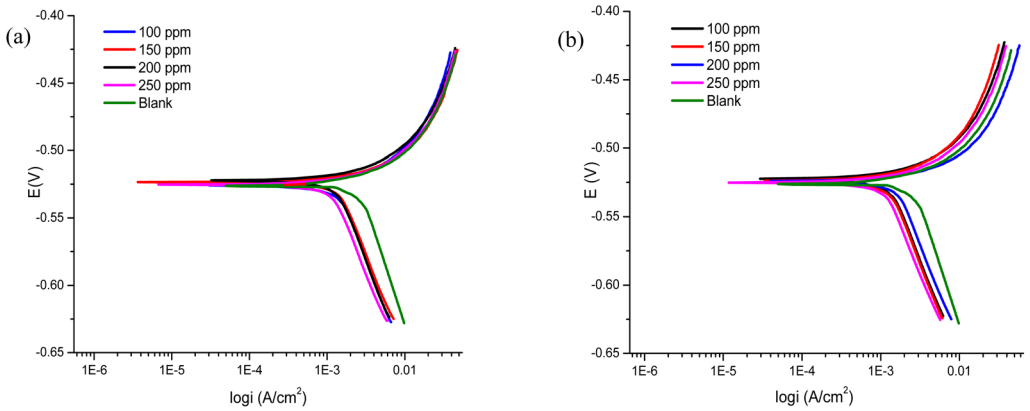

Fig. 8 Curves of PDP technique for corrosion of Al in 1 M HCl in the presence and absence of specific concentrations from (a) SCS and (b) GPP extracts at 25 °C.

Table 7 PDP parameters for Al corrosion in 1 molar HCL in the non-existence and the existence of changed doses of SCS and GPP extracts at 25 °C

Conc. (ppm)	$-E_{corr}$ (mV)	I_{corr} (mA cm^{-2})	β_a (mV)	$-\beta_c$ (mV)	θ	% I.E.
SCS extract						
Blank	524.89	2.800	43.87	177.78		
100	525.70	1.385	27.98	141.15	0.505	50.5
150	523.80	1.356	24.46	146.83	0.516	51.6
200	521.46	1.283	21.37	156.13	0.542	54.2
250	525.32	1.121	21.61	152.45	0.600	60.0
GPP extract						
Blank	524.89	2.800	43.87	177.78		
100	522.75	1.310	30.85	146.40	0.532	53.2
150	523.61	1.245	28.96	150.59	0.555	55.5
200	524.03	1.232	18.26	132.76	0.560	56.0
250	524.82	1.058	23.13	143.46	0.622	62.2

The adsorbed molecules forming a protective film, which were investigated at the interfacial region between the solution and the aluminum surface, raise the charge-transfer impedance without altering the impedance behavior. Using the polarization measurements indicated the same findings, that the electrochemical reaction mechanism remains similar with the addition of both extracts. The dissolution of Al metal is slowed down by the exchange of adsorbed water molecules with SCS and GPP extract particles on the aluminum surface.[17] The % I.E. deduced from the WL and PDP experiments is quite close to what has been found from the EIS measurements.

Room temperature efficiencies of 60–70% are within a reasonable range of those of known green inhibitors in strong acids and can be deemed to be acceptable to an environmentally friendly system.[72,73] The electrochemical behavior of the aluminum electrode, both with and without the addition of SCS and GPP inhibitors, is characterized using Bode diagrams (impedance magnitude $|Z|$ and phase angle *vs.* frequency). These plots offer a comprehensive view of the system by incorporating frequency-dependent data. Fig. 11 shows the Bode plot in the absence and presence of SCS and GPP extract at 25 °C for Al. The graphical data indicates a direct correlation between higher inhibitor concentrations and an increase in the phase angle. This shift suggests a reduction in capacitive behavior at the metal's surface, which effectively suppresses the rate of metal dissolution.[57] The rise in peak heights associated with higher inhibitor concentrations suggests an enhanced capacitive response at the metal–solution interface. This phenomenon is attributed to the adsorption of inhibitor molecules, which results in corrosion inhibition. Consistent with the findings from weight loss and potentiodynamic polarization techniques, the EIS data confirms that SCS and GPP extracts act as effective corrosion inhibitors.

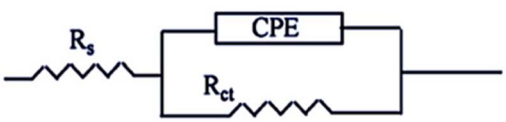

Fig. 9 Illustration of an equivalent circuit for measuring EIS data.

4.6. Atomic force microscope (AFM) analysis

Employing atomic force microscopy, the previous results were validated. To examine the corrosion morphology of Al metal in

Table 8 Data obtained from EIS technique for Al corrosion in 1 M hydrochloric acid at specific concentrations of inhibitors at 25 °C

Conc. (ppm)	R_{ct} (Ω cm^2)	R_s (Ω cm^2)	$Y_0 \times 10^5$ (Ω^{-1} S^n cm^{-2})	n	$C_{dl} \times 10^5$ (F cm^{-2})	θ	% I.E.
SCS extract							
Blank	10.970	1.710	7.491	0.980	7.640		
100	23.119	1.818	8.688	0.975	7.410	0.525	52.5
150	23.702	2.202	8.242	0.980	7.300	0.537	53.7
200	26.567	2.008	8.447	0.972	7.080	0.587	58.7
250	29.001	1.849	9.121	0.969	6.690	0.622	62.2
GPP extract							
Blank	10.970	1.710	7.491	0.980	7.640		
100	21.219	1.730	8.532	0.957	6.422	0.483	48.3
150	25.358	2.398	8.320	0.957	6.310	0.567	56.7
200	26.385	2.619	7.893	0.986	6.143	0.584	58.4
250	30.197	2.220	8.698	0.962	6.058	0.637	63.7

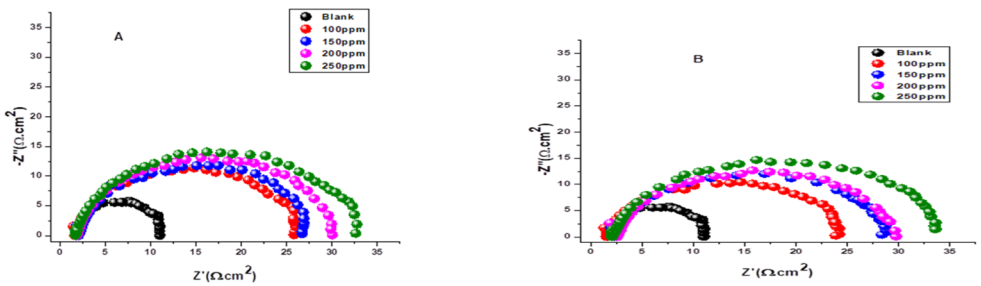

Fig. 10 Nyquist plots for aluminum in 1 M HCl without and with specific concentrations of inhibitor (A) SCS and (B) GPP extracts at 25 °C.

1 M hydrochloric acid, whether the higher concentration (250 ppm) of inhibitors is present or not, AFM analysis was performed on the samples post a 6 hour immersion period. In order to expose the metal samples for morphological assessment of the surface roughness, the metal sheets were first polished, thoroughly rinsed using distilled water, and subsequently gently dried. Three Al samples were presented in Fig. 12.

The findings of this examination are summarized in Table 9. The root-mean square roughness, indicated by S_q, indicates the root mean square of the height deviancies measured from the mean plane within the sampling area. The average roughness, implied by S_a, displays the average deviation of the roughness profile at each position from a mean plane over the sampling area. The maximum peak-to-valley height (P–V), the distance in height between the lowest valley and the highest peak in the sampling area, is also employed. The average roughness of the aluminum surface dropped from 70.052 to 25.211 nm and also to 51.996 nm when it was immersed in the acid with 250 ppm of SCS and GPP extracts, respectively. The metal surface was smoothed, and uniform corrosion was hindered by the highest concentration from both extracts; however, SCS works better than GPP. As the extracted SCS and GPP particles adsorbed onto the surface, they caused a decrease in the interaction that existed between the Al and HCl acid.

4.7. X-ray photoelectron spectroscopy (XPS) examination

The nature of SCS and GPP extract adsorption was illustrated by analyzing the buildup of a film of the extract molecules over the aluminum surface using the XPS technique in HCl medium. Fig. 13, 14, and 15 show the XPS decomposition spectra of the individual elements that exist in the layers deposited on the surface after submerging in a solution enriched with the extracts of SCS and GPP. The elemental binding energies documented on the characterization of XPS spectra for superficial layers in publications and the literature are used to interpret all of the obtained spectra.[74] As illustrated in Fig. 13, 14, and 15, the XPS spectra, recorded for Al post immersion in HCl acid (1 M) containing 250 ppm of SCS or GPP extract, are composed of the components Al 2p, Cl 2p, O 1s, and C 1s. The binding energies, along with the similar interpretation of each peak, are listed in Table 10.[64]

In 1 M HCl solution and 250 ppm of SCS extract, the Al 2p, Cl 2p, C 1s, and O 1s spectra of aluminum were seen. Four distinct peaks were found in C 1s spectra exhibiting binding energies (BE) of 284.365, 285.7, 287.918, and 289.5 eV. The O 1s spectra showed three distinct peaks having binding energies of around 530.5, 532.041, and 534.5 eV. Also, in 1 M HCl solution and 250 ppm of GPP extract, the Al 2p, Cl 2p, C 1s, and O 1s spectra of aluminum were observed. Four consecutive peaks were found at binding energies of 284.469, 286.7, 287.917, and 289.5 eV in C 1s spectra. The O 1s spectra showed three distinct peaks having binding energies of 530.5, 532.025, and 534 eV. The adsorption process of SCS and GPP extracts on the aluminum surface in HCl solution can be validated by the XPS data.

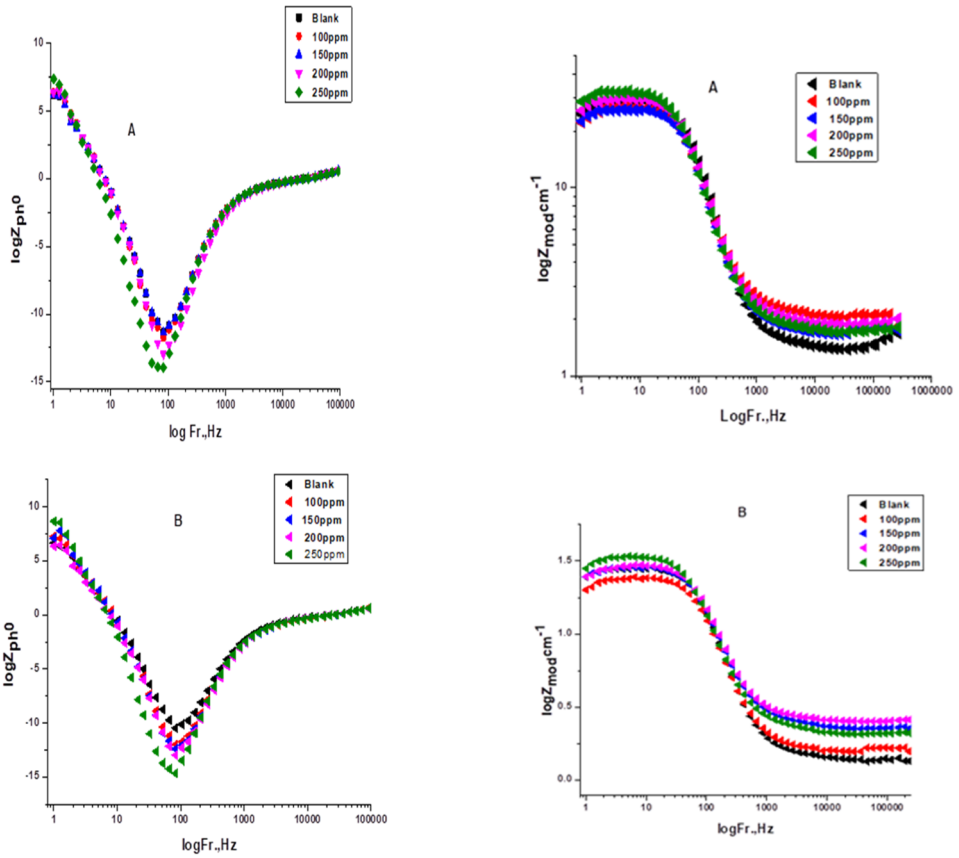

Fig. 11 Bode charts for liquefaction of Aluminum in HCl attendance and absence of changed doses of (A) SCS and (B) GPP extract at 25 °C.

4.8. Quantum chemical calculations

Adsorption of phytochemical compounds on the aluminum surface serves as the reason for the inhibitory effect of SCS and GPP extracts. Molecular dynamics simulations and quantum chemical parameters were employed to point out the distinct contributions made by multiple individual compounds in the extracts. Tables 11 and B5 (SI) display the optimal geometric structure (neutral and protonated) of the LUMO and HOMO orbitals of key components in SCS and GPP extracts. The HOMO orbital of (+)-catechin in its neutral and protonated form is primarily observed at the oxygen atoms and cyclic hydrocarbon, but the LUMO orbital is largely distributed at the other benzene ring substituted with two hydroxyl groups at adjacent positions. The carbon and oxygen atoms in caffeic acid (nearly the entire compound) are where the LUMO and HOMO orbitals are to the greatest extent scattered, in either neutral or protonated states.

The HOMO orbital of chlorogenic acid is spread at the benzene ring substituted with two hydroxyl groups at adjacent positions in addition to the adjacent carbons in its neutral and protonated form, but the LUMO orbital is mostly distributed at the carbon atoms in its neutral form in addition to the carbonyl group in its protonated form. Some of the components in neutral or protonated form, the HOMO and LUMO orbitals, are dispersed across almost the entire compound, like ferulic acid, gallic acid, kaempferol, *p*-coumaric acid, quercetin, vanillic acid, and protocatechuic acid. When apigenin is neutral or protonated, the HOMO and LUMO orbitals are spread throughout the entire compound, but in protonated form HOMO orbital is distributed on oxygen atoms and cyclic hydrocarbons. In the case of melitidin, 2,2′-methylenebis, and quercetin triglucoside, the HOMO and LUMO orbitals are distributed around carbons and oxygen in some hydrocarbon rings in the neutral and protonated forms. The LUMO orbital of myricetin and *p*-OH benzoic acid is spread throughout the entire compound in its neutral and protonated forms, while the HOMO orbital is dispersed throughout the entire compound in the neutral form and spread at some carbon and oxygen atoms in its protonated form. According to naringenin, the HOMO and LUMO orbitals are spread throughout the carbon in the rings and oxygen atoms attached to it in neutral or protonated form.

Although higher E_{HOMO} data reflect that the compound has a greater capability to deliver electrons to the vacant p-orbital on the aluminum surface, lower E_{LUMO} values imply that the capability of these molecules to receive electrons.[75] The E_{HOMO} and E_{LUMO} data illustrated in Tables B6 and B7 (SI) indicate that the compounds that were extracted from SCS and GPP that have been examined have the capability to provide and receive electrons. Quercetin and (+)-catechin in the non-protonated form have the highest E_{HOMO} values (less negative) in SCS extract, according to Table B6 (SI), suggesting that they have the best corrosion inhibition (check out also Fig. 16). Also, 2,2′-

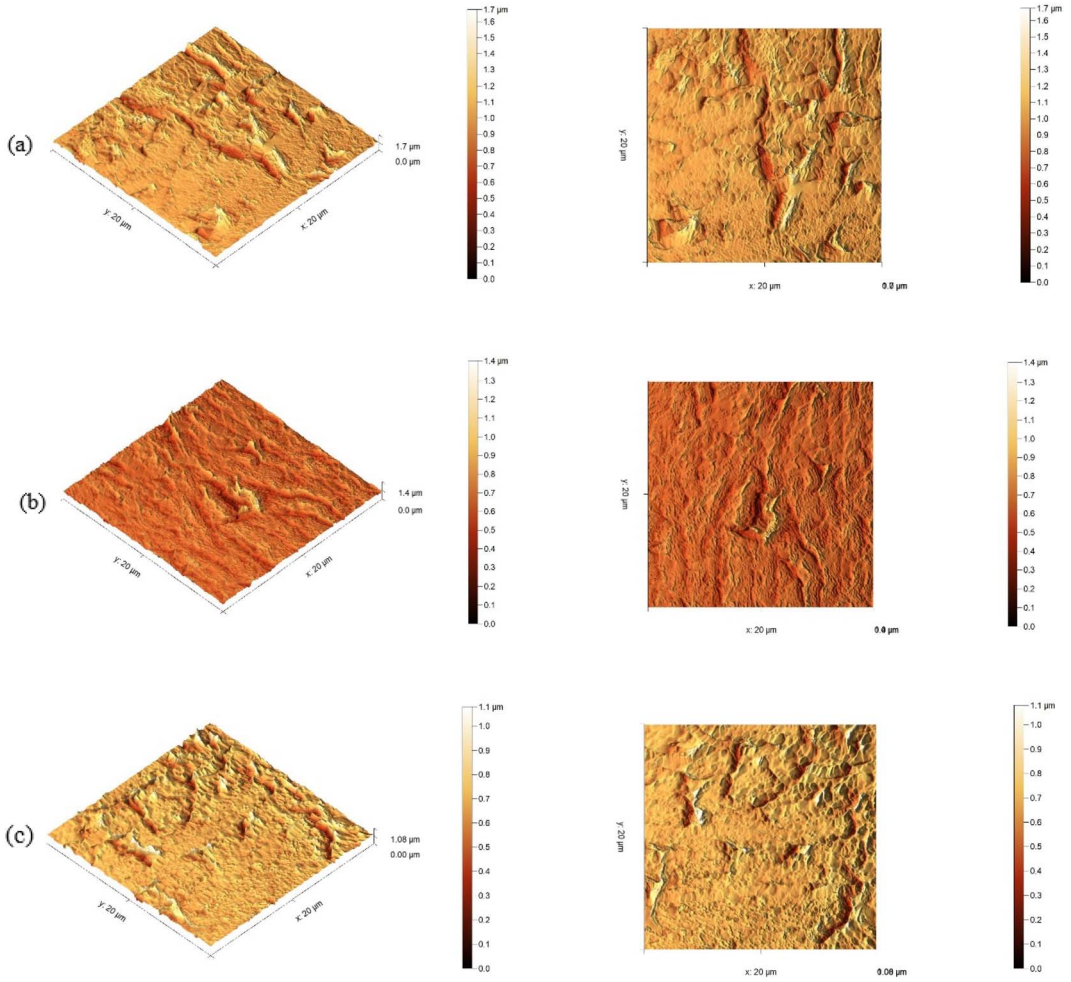

Fig. 12 The surface of the Al electrode after 6 hours of immersion in a 1 M HCl solution (a) in the absence of the inhibitors, (b) having 250 ppm SCS, and (c) having 250 ppm GPP.

Table 9 The surface morphological data of aluminum after 6 hours immersion in a 1 M HCl solution, either with or without 250 ppm of SCS and GPP

Samples	S_q (nm)	S_a (nm)	Maximum peak-to-valley height (nm)
Aluminum in 1 M HCl	105.818	70.052	1675.3
Al + 1 M HCl + 250 ppm SCS	44.708	25.211	1392.5
Al + 1 M HCl + 250 ppm GPP	77.120	51.996	1079.1

methylenebis is an excellent inhibitor molecule in GPP extract, according to its high E_{HOMO} value (Fig. 17).

The energy gap represents another critical factor that demonstrates the adsorption reactivity of the molecules. The ΔE value is inversely correlated to the adsorption reactivity. A lower value of ΔE is an indication of a good inhibitor molecule, as it indicates that less energy of ionization is necessary to liberate an electron out of the external shell orbital. Fig. 16 and 17 demonstrate that most of the compounds in the protonated form of both extracts have a lower energy gap than that of the non-protonated and vacuum forms, demonstrating that the extract adheres more strongly to the aluminum surface in the protonated state. Softness of the inhibitor molecules contributes significantly to the quick transmission of electrons to the acceptor. Consequently, softer molecules react more easily in contrast to those with greater hardness.[76] Adsorption may be limited to the portion of the molecule having the greatest magnitude for the smoothest transfer of electrons.

Dipole moment is an important property that is used as an index to identify the corrosion inhibition direction. It functions as an indicator of the polarity of the bond in accordance with electron distribution within the investigated molecule. The large value of the dipole moment is considered a reflection of the effective adsorption of the molecule to the Al surface;

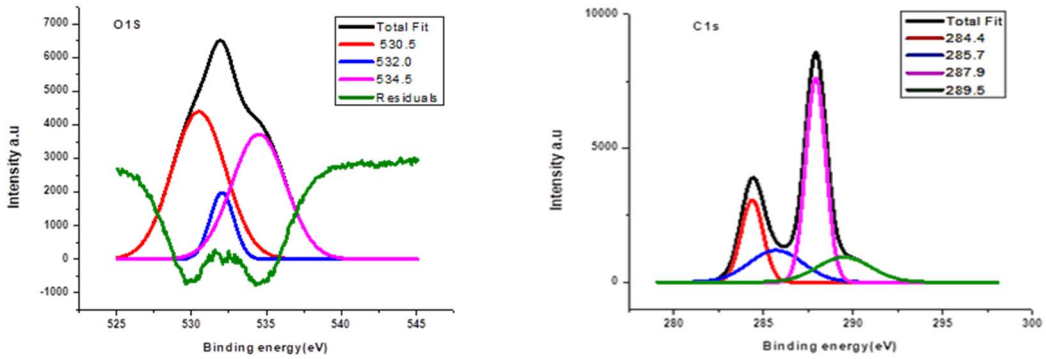

Fig. 13 XPS results from scanning elements, C 1s, and O 1s at 1 M HCl with 250 ppm for SCS extract.

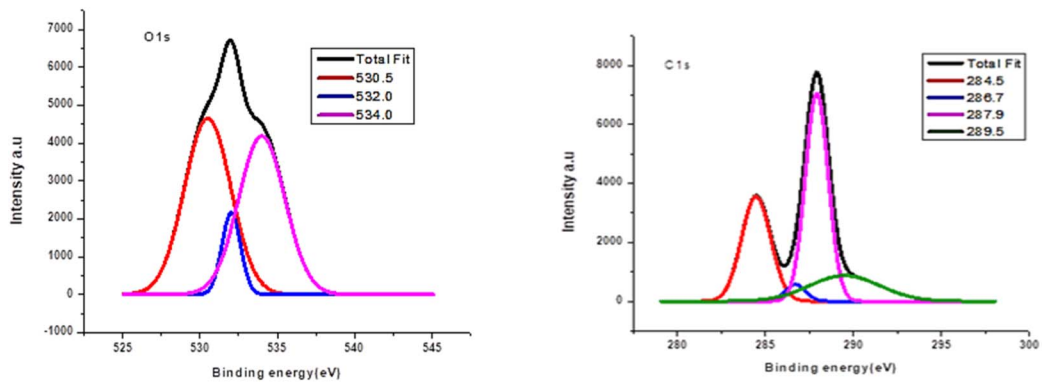

Fig. 14 XPS results from Scanning elements, C 1s, and O 1s at 1 M HCl with 250 ppm from GPP extract.

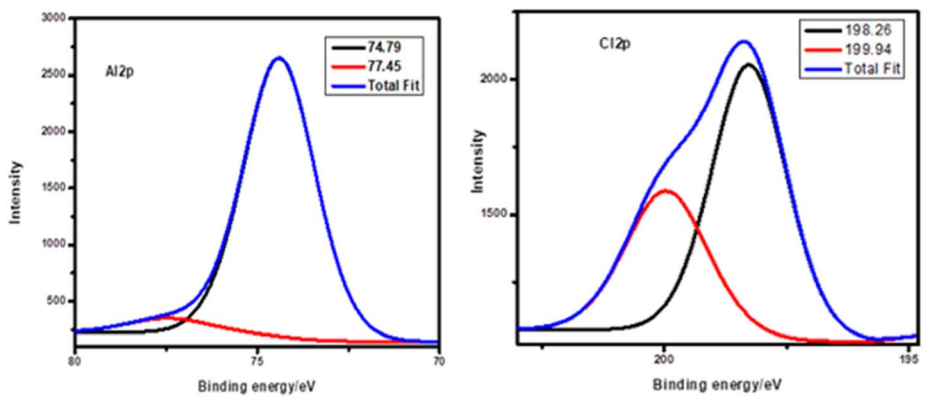

Fig. 15 XPS results from Scanning elements, Al 2p and Cl 2p of aluminum at 1 M HCl with 250 ppm extract.

moreover, there is better % I.E. on a consequence of the strong dipole–dipole interaction on the Al surface.[77] Measured dipole moments revealed a significant change in value in protons, indicating that SCS and GPP extracts are tightly bonded to the aluminum surface, especially in the proton form. The compound in the SCS extract that is better able to attach to the aluminum surface due to the strong dipole moment of the protonated form is *p*-coumaric acid, and that in the GPP extract is quercetin triglucoside.

The increase in the electron-donating capacity of the investigated inhibitors to the aluminum metal surface has been estimated to elevate inhibition efficiency whenever ΔN is below 3.6.[78] From the results included in Tables B6 and B7 (SI), the positive value of ΔN indicates the inhibitor's capability to transfer electrons to the Al surface, while $\Delta N < 0$ is owing to back-donation from the metal surface to the inhibitor molecules.[79] Electronegativity (χ) reflects the extent to which an electron can attract molecules of an inhibitor. Significant pull force to withdraw the electron from the aluminum surface is

Table 10 The binding energies (eV) for the significant core lines presented on the aluminum surface that SCS and GPP handle

		1 M HCl	
	Core element	BE (eV)	Assignments
SCS extract	C 1s	284.365	C–C/C–H
		285.7	C–O
		287.918	C═O
		289.5	O–C═O
	O 1s	530.5	O–C
		532.041	O═C
		534.5	O–H
	Al 2p	74.43	Al_2O_3
		77.45	$Al(OH)_3$
	Cl 2p	198.26	Cl $2p_{3/2}$
		199.94	
GPP extract	C 1s	284.469	C–C/C–H
		286.7	C–O
		287.917	C═O
		289.5	O–C═O
	O 1s	530.5	Metal oxide
		532.0258	Hydroxyl/defect
		534	Organic/adsorbed
	Al 2p	74.43	Al_2O_3
		77.45	$Al(OH)_3$
	Cl 2p	198.26	Cl $2p_{3/2}$
		199.94	

indicated by higher values of χ_{inh}. Therefore, inhibitor molecules with higher electronegativity values act as electron acceptors, while lower values are an indication of electron donation. Inhibitor molecules with lower χ_{inh} donate electrons easily, and a higher inhibition level is achieved.[80]

Larger molecules of SCS and GPP extracts provide a better inhibitory effect because they increase the space at which those molecules can adhere to the aluminum surface. In light of this, Al surfaces could bind to SCS and GPP extracts more effectively, thereby inhibiting corrosion. Corresponding to the nucleophilicity index (ε), as the value increases, it gives an indication about how well the molecule can facilitate the adhesion of electrons into the aluminum surface. From the results included in Tables B6 and B7 (SI), the observation is that the vacuum form of all compounds in SCS and GPP extracts has a greater value of the nucleophilic index.

The ability of SCS and GPP molecules to transmit or receive electrical charge has recently been assessed using the electro-donating power (ω^-) and the electro-accepting power (ω^+). Good electron donor molecules are indicated by low ω^- values. Good electron acceptors have high ω^+ values.[81] As illustrated in the results, $\omega^- > \omega^+$ for all SCS and GPP compounds, which emphasizes that the donating power is in control. This is an indication that the molecules have a significant binding to the aluminum surface aimed at avoiding corrosion. A positive hardness value, along with negative back-donation energy values, indicates the transfer of electrons and charge donation from aluminum to the SCS or GPP molecules.

4.8.1. Fukui indices and Mulliken charge. The position of the donor and acceptor atom of the active adsorption center in the inhibitor's molecule is estimated using Fukui indices and the Mulliken charge analysis. The donor and acceptor active centers within the compounds of SCS and GPP extracts serve as the sites that are the most prone to adsorb onto the aluminum surface. The findings of Mulliken charges for both extracts in neutral, protonated, and vacuum form are summarized in Table B8 (SI). The positive and negative values of the Mulliken charge highlight how the donor–acceptor active sites within the compounds of SCS and GPP extracts boost the sensitivity of these compounds to aluminum atoms. According to the results tabulated in Table B8 (SI) and displayed in Fig. 18, a comparison was done based on the total negative charge (TNC). It results from the sum of all negative charges throughout the molecule. It is obvious that as the inhibitor molecules were protonated, the total negative charge increased (less negative) and acted as an attractor. The organic compounds that may possess one or more heteroatoms protonate easily at such sites under the acidic conditions, like hydrochloric acid, which results in the formation of molecules with a positive charge. These lead to interaction with the widely dispersed anions as Cl^- ions. This can illustrate how protonation can affect the local centers of the inhibitor's compounds. Compared to the other compounds, quercetin triglucoside and chlorogenic acid have a higher electron-donating capacity and the highest TNC value, leading to the highest inhibition efficiency.[82,83]

The atoms in the investigated molecules with greater values of the Fukui index (f_K^+ and f_K^-) are shown in Fig. 19 for myricetin and Fig. A5 (SI) for the other compounds of both extracts in protonated, non-protonated, and vacuum forms. The findings show that every molecule possesses distinct atoms responsible for nucleophilic and electrophilic behavior. The atom within the molecule having the biggest f_K^+ value is the most preferable site for nucleophilic attack, which has a relation with the LUMO part and, as a consequence, enhances the ability to react to donor reagent. On the other side, the atom within the molecule having the biggest f_K^- value is the most preferable site for electrophilic attack, which is observed in conjunction with the HOMO part, resulting in enhancement in the ability to react in the direction of an acceptor. The value of f_K^- for atoms was observed to decrease in protonation as a result of obstruction done by H^+ to these centers, leading to a decrease in donor property. Also, f_K^+ values for atoms were increased as a consequence of the ability of atoms toward electron acceptance. Furthermore, it is observed that certain atoms within the same compound have greater values of f_K^-, while others have higher f_K^+ values. This indicates that the same compound has a dual effect, as it can receive and give electrons.[84]

4.8.2. Electrostatic potential of molecules (MESP). The molecular electrostatic potential served to indicate the location of chemical reactions. The electrostatic potential has distinct colors at different positions in the regions where electron density is distributed, as shown in Tables 12 and B9 (SI). The red color is an indication of an electrophilic zone that is electrically active; it lies in a region of predominantly negative electrostatic potential. The blue color refers to the nucleophilic zone in which predominantly positive electrostatic potential is

Table 11 The HOMO and LUMO orbital distribution and molecular structure optimization for important components in SCS and GPP extracts were assessed *via* the DMol^3/GGA/BOP approach (neutral)

Compound	Optimized structure	HOMO	LUMO
(+)-Catechin	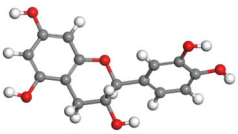	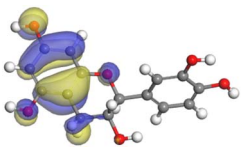	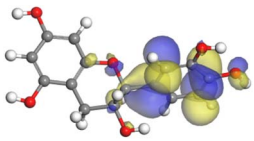
Caffeic acid	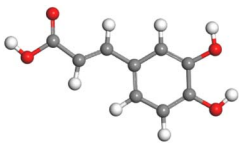	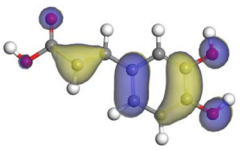	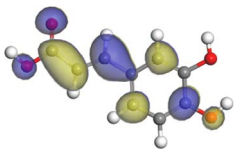
Chlorogenic acid	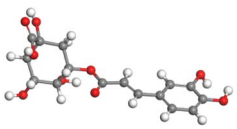	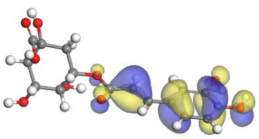	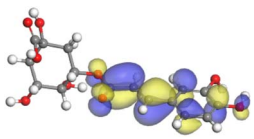
Ferulic acid	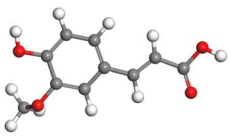	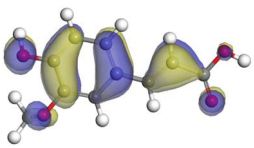	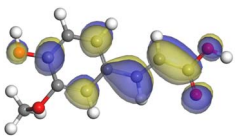
Gallic acid	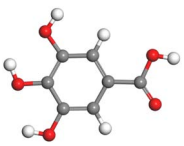	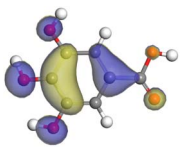	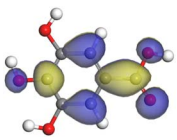
Kaempferol	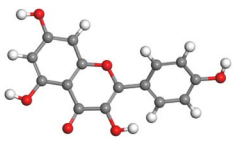	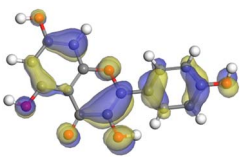	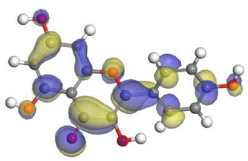
Myricetin	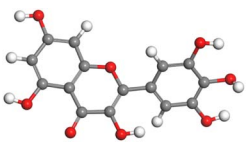	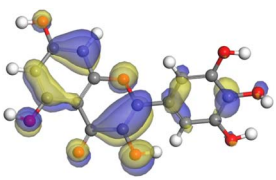	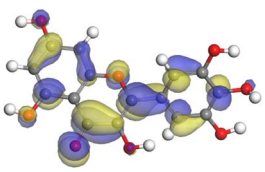
p-Coumaric acid	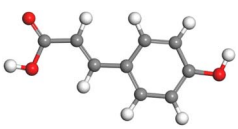	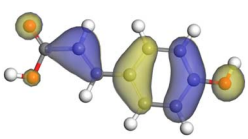	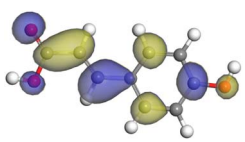
p-OH benzoic acid	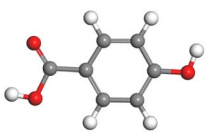	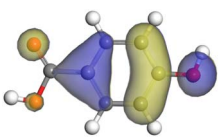	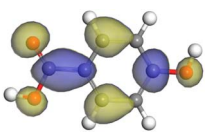
Protocatechuic acid	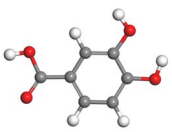	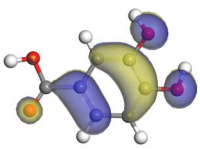	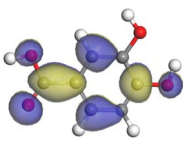

Table 11 (*Contd.*)

Compound	Optimized structure	HOMO	LUMO
Quercetin	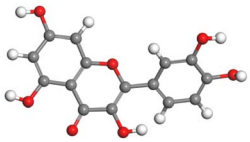	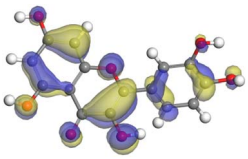	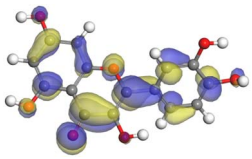
Syringic acid	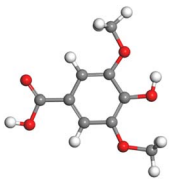	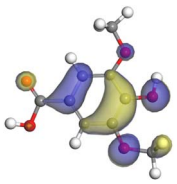	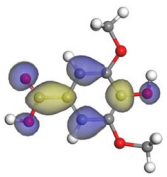
Vanillic acid	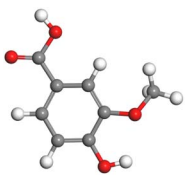	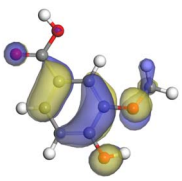	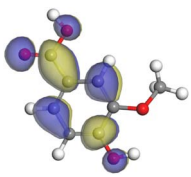
Naringenin	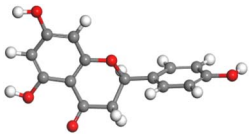	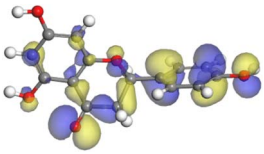	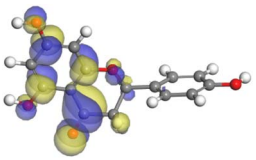
Epigallocatechin	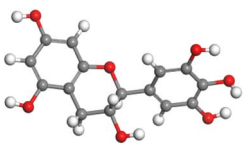	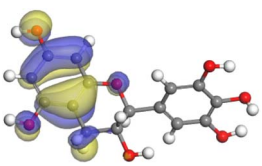	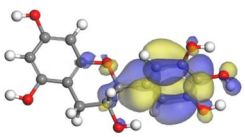
Apigenin	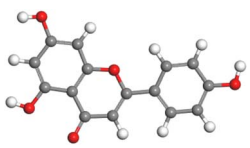	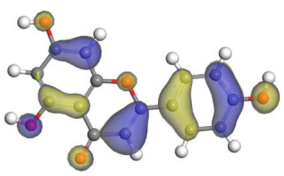	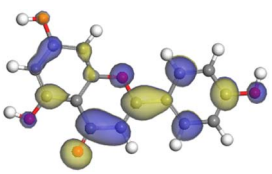
Quinic acid	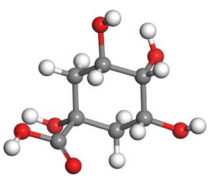	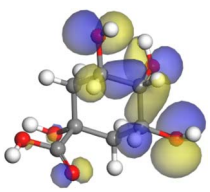	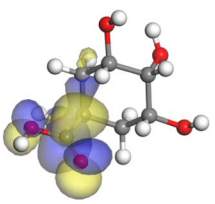
Melitidin	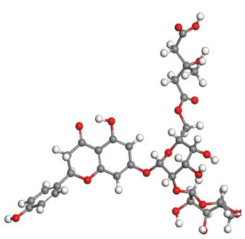	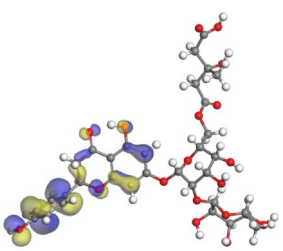	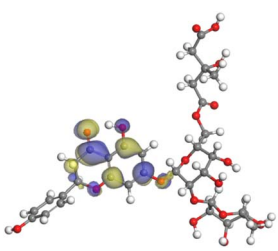

Table 11 (*Contd.*)

Compound	Optimized structure	HOMO	LUMO
2,2′-Methylenebis	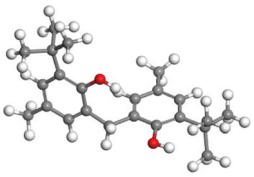	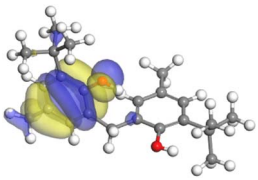	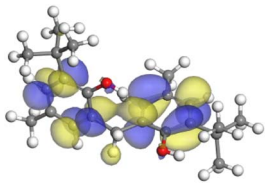
Quercetin triglucoside	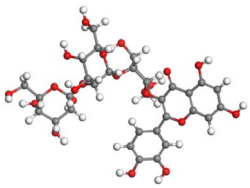	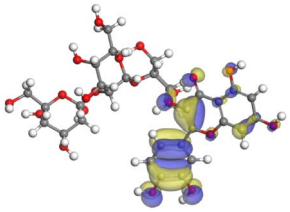	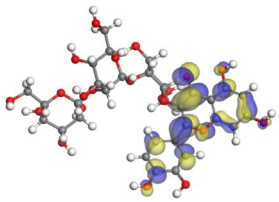

obtained; green spaces indicate places where there is less likelihood. The electron-dense regions mostly contain heteroatoms and double conjugate bonds. The presence of oxygen is an indicator of electrophilic attack in the negative zones. Hydrogen atoms that are blue in hue encourage nucleophilic attacks.

4.9. Molecular dynamic simulations

The adsorption locator was adopted to determine the optimal prearrangement for the inhibitor molecule (the adsorbent) over the Al (1 1 1) substrate in the corrosion-simulating fluid (250H_2O molecules plus 10H_3O^+ and 10 Cl^-). The plan and side views taken to Al (111) substrate demonstrate the adsorption processes of the SCS and GPP molecules in their neutral, protonated, and vacuum forms as illustrated in Tables 13 and B10 (SI), respectively.

The outcomes from the molecular dynamic simulation, such as the deformation energy, the total energy, and the rigid adsorption energy, are listed in Tables 14, B11, and B12 (SI). The summation of the rigid and deformation energy is presented by the adsorption energy. The rigid adsorption energy is defined as the energy released due to the adsorption of unrelaxed molecules on the substrate surface (before the geometry optimization). While the deformation energy is defined as the energy required to deform the molecules during adsorption to adapt well to the surface. dE_{ads}/dN_i is a representation of the energy gained throughout the separation of an individual adsorbate particles out of the adsorbent substrate, and a higher negative value is an indication of the spontaneity of the adsorption. It is obvious that the adsorption of SCS and GPP components is stronger than water, as shown by the values for the inhibitor components being higher than those for water molecules.[79] The SCS and GPP components are therefore expected to be adsorbed on the aluminum surface, creating a resistive film, which resists the HCl acid attack on the Al surface.

Upon close examination, the molecular arrangement of the inhibitor molecules is found to be almost parallel and very close to the aluminum surface. The components of SCS and GPP extracts shall employ this adsorption characteristic for expanding the aluminum's contact area or surface covering capabilities. As the aluminum/SCS or GPP extract contact zone is large, this will restrict the access to the substrate and prevent the undesired chloride anion attack. The direction of electron transfer is reversed, from the aluminum surface to the constituents of both extracts, in the case of a charged proton component causing the reaction to change back. The metal surface is protected from the acidic solution corrosion by the strong adsorption of SCS or GPP extract components, which provide a strong adsorbent film. SCS or GPP extract molecules were shown to adsorb in an acidic (neutral or proton) and a vacuum system. The more efficient adsorption of SCS or GPP extract molecules on the aluminum surfaces is demonstrated by the elevated negative adsorption energies in the existence of an aqueous solution as compared with their counterparts in the vacuum.

4.10. Corrosion inhibition mechanism

It is observed that increasing the concentration of SCS and GPP extracts leads to a gradual decrease in the metal corrosion rate and a corresponding increase in inhibition efficiency. As observed from weight loss results, Al dissolution in the corrosive solution occurs at a slow rate initially and increases over time. This behavior can be attributed to the presence of a pre-existing Al_2O_3 film remaining on the metal surface. Exposure of the free aluminum surface to acid solutions leads to corrosion and subsequent structural deterioration. Aluminum undergoes several sequential electrochemical reactions when exposed to an acidic environment:[85]

$$Al_2O_3 + 3H_2O \rightarrow 2Al(OH)_3$$

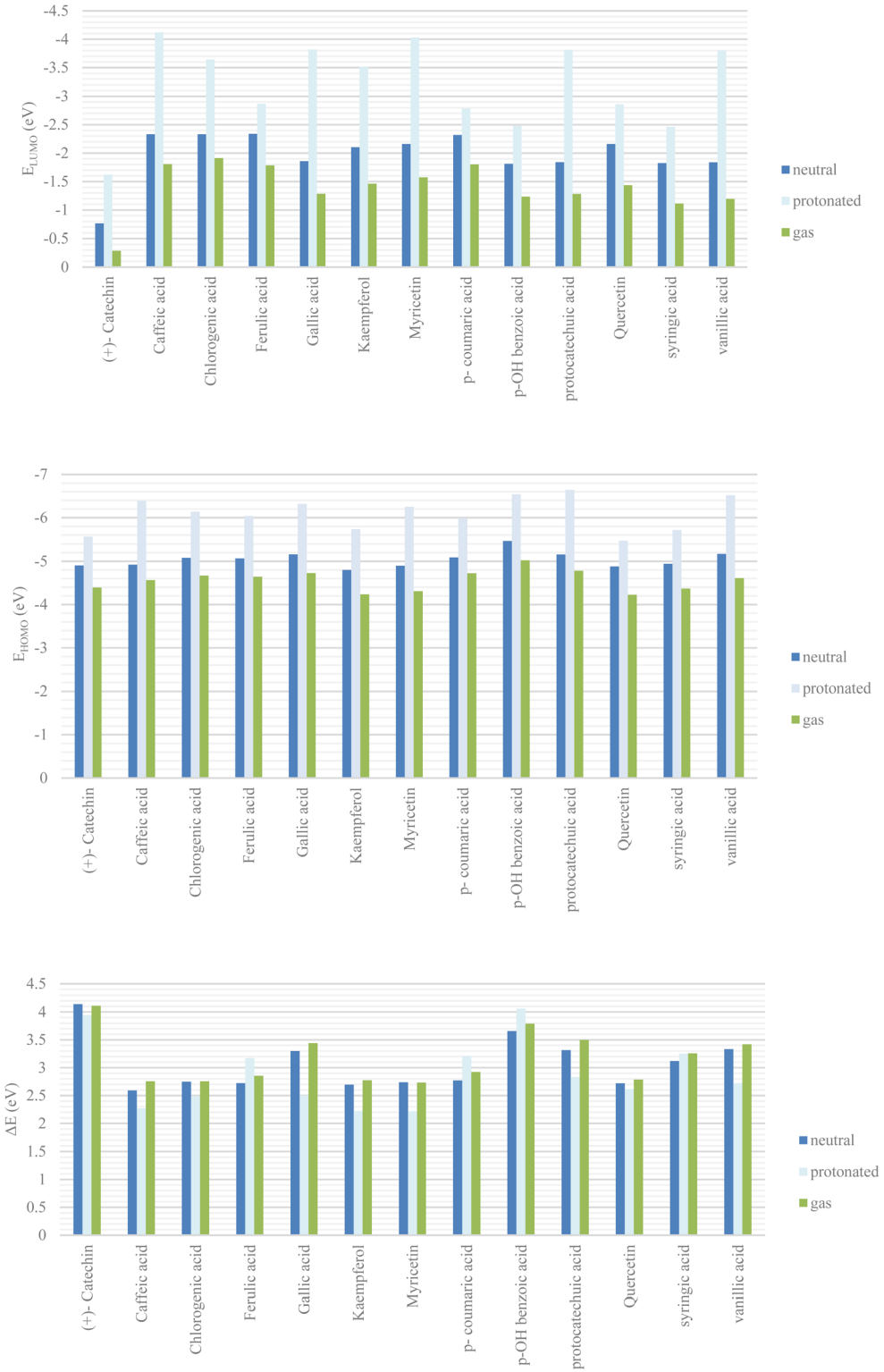

Fig. 16 E_{HOMO}, E_{LUMO}, and ΔE values for studied compounds in SCS extract.

$$Al(OH)_3 + H^+ \rightarrow Al(OH)_2^+ + H_2O$$

$$Al(OH)_2^+ + 2H^+ \rightarrow Al^{3+} + 2H_2O$$

Overall reaction: $Al_2O_3 + 6H^+ \rightarrow 2Al^{3+} + 3H_2O$

Al^{3+} exists as $Al[(H_2O)^6]^{3+}$ in acid solution

In hydrochloric acid, the corrosion process initiates when chloride ions adsorb onto the active sites of the aluminum surface, thereby making the oxide layer suspectable to dissolution.[86] As the oxide layer is destabilized from the surface,

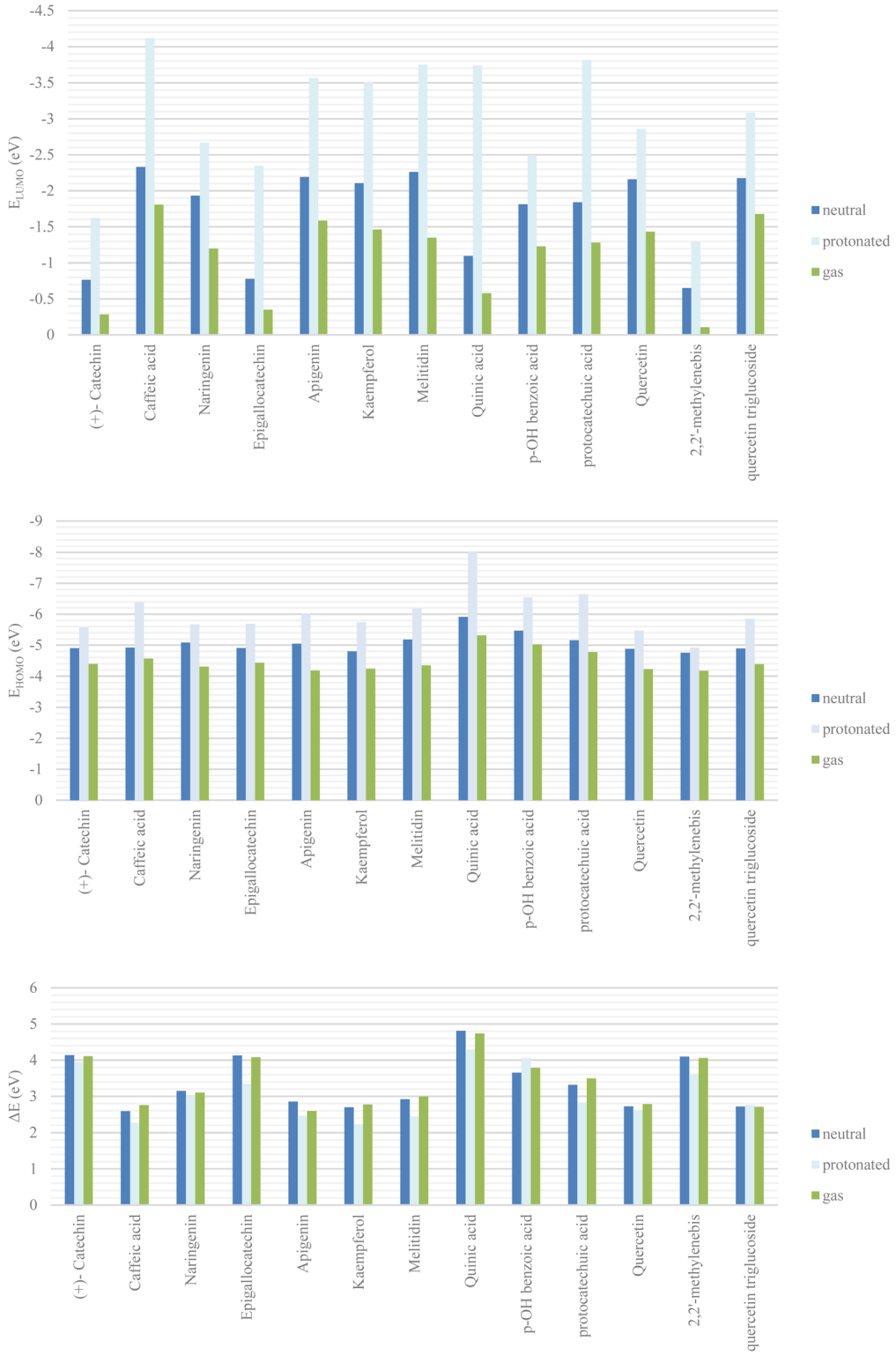

Fig. 17 E_{HOMO}, E_{LUMO}, and ΔE values for studied compounds in GPP extract.

a positive charge is formed causing Cl^- ions attraction and increase the corrosion process. This phenomenon affects the reactivity over the Al surface as the un affected sites serve as cathodic regions.[86] These cathodic regions, facilitating reduction reaction, along with the anodic sites increase the corrosion rate of Al.

As reported in previous studies, inhibitor particles largely adhere to the aluminum surface through physical and/or chemical adsorption mechanisms. The compounds of the

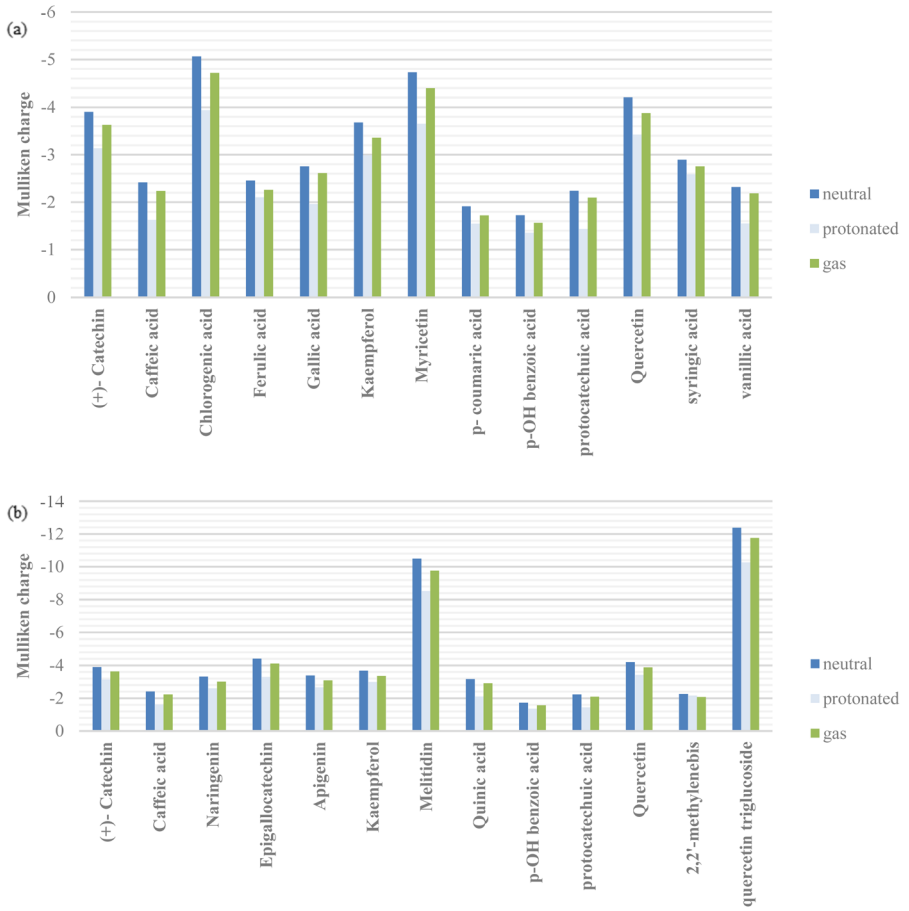

Fig. 18 Protonated, non-protonated, and vacuum molecules in (a) SCS and (b) GPP extract and their TNC.

extracts in HCl solution, may found in their neutral form or in the form of protonated cations. The above findings confirm that the inhibitor is adsorbed on the aluminum surface. In the literature, four mechanisms have been proposed to describe the adsorption of inhibitors at the metal–solution interface. These mechanisms include: (i) electrostatic attraction between charged inhibitor molecules and the charged metal surface; (ii) coordination through unshared electron pairs on the inhibitor; (iii) interaction of π-electrons within the inhibitor molecule with the metal; and (iv) a combined mechanism of (i) and (iii).[87]

In 1 molar HCl solution, the aluminum oxide film which has a positive charge attracts chloride ions. The attachment of the inhibitor molecules to the Al surface is driven by their electronegative oxygen atoms, the π electrons within their aromatic rings, or the cooperative contribution of these two functional groups. Because of this, protonated inhibitors are more likely to

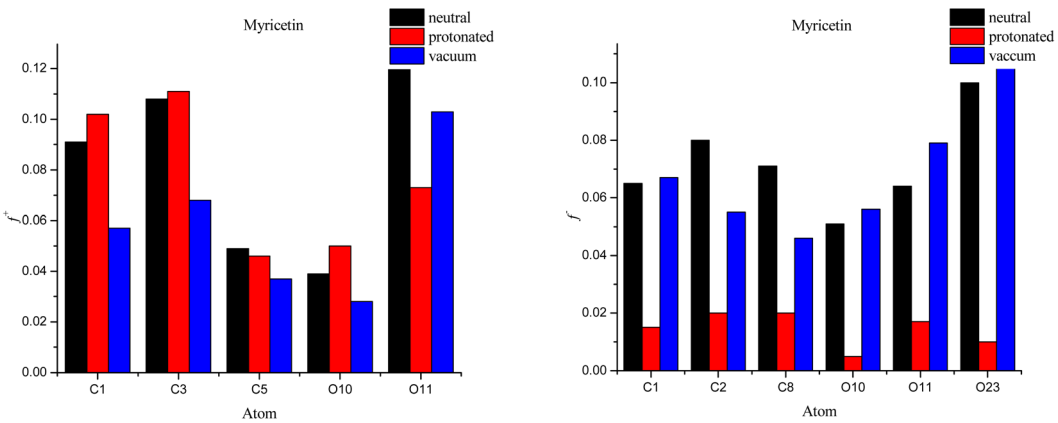

Fig. 19 A graphical depiction of myricetin's Fukui indices for its more reactive atoms in both their protonated and non-protonated systems.

Table 12 Images illustrate the protonated and non-protonated molecule electrostatic potentials, along with the inhibitor's electrostatic contour

Plant	Compound	Neutral	Protonated
		Maximum density ← → Minimum density	
SCS&GPP	(+)-Catechin	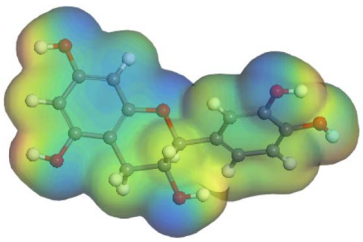	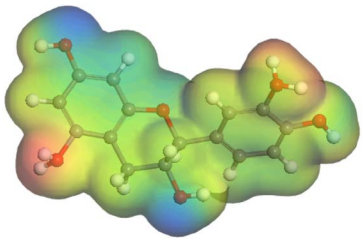
SCS&GPP	Caffeic acid	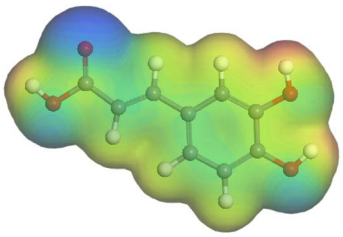	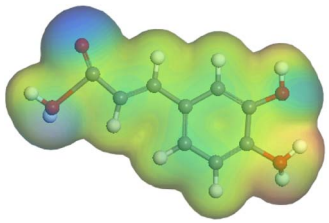
SCS	Chlorogenic acid	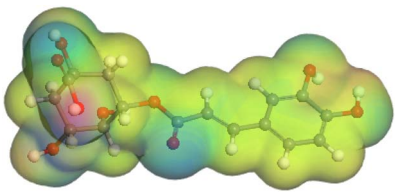	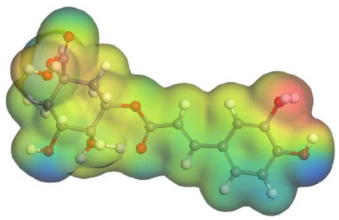
SCS	Ferulic acid	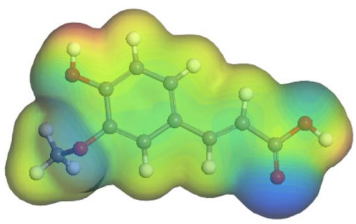	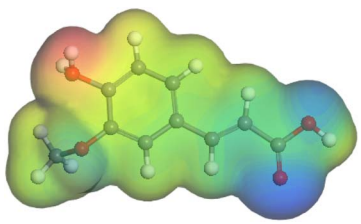
SCS	Gallic acid	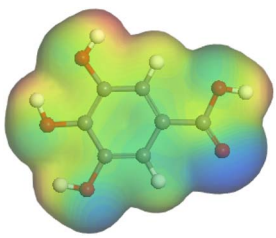	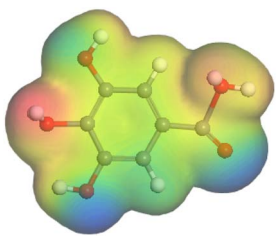
SCS&GPP	Kaempferol	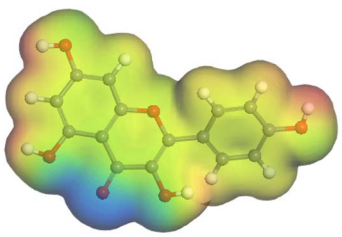	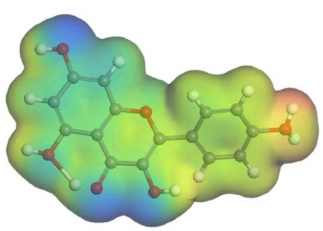

Table 13 The adsorption locator module's recommendation for some of the best formation for the adsorption of SCS and GPP extracts on aluminum (1 1 1)

Compound		Top view	Side view
(+)-Catechin	neutral	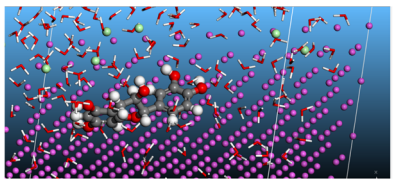	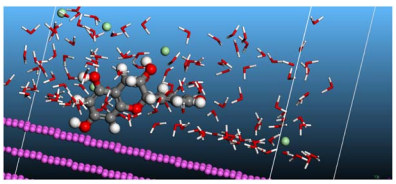
	protonated	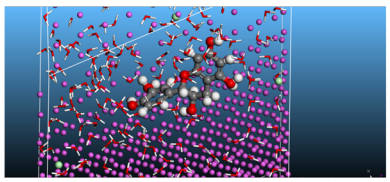	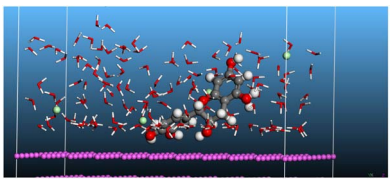
	vacuum	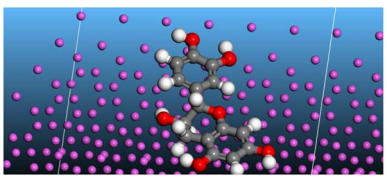	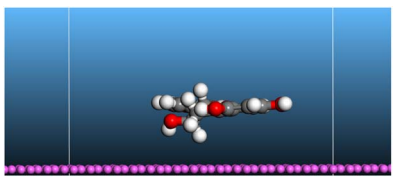
Caffeic acid	neutral	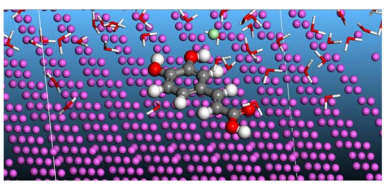	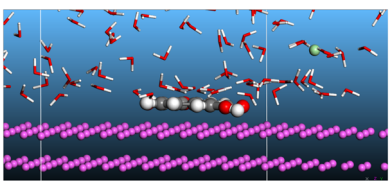
	protonated	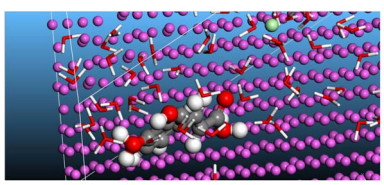	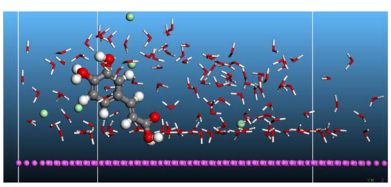
	vacuum	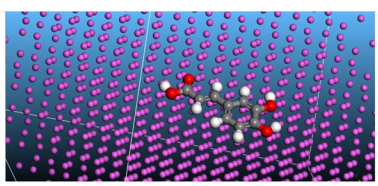	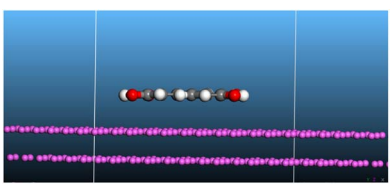

physically adhere onto the Al surface as a result of electrostatic attraction, where the positively charged inhibitor molecules are drawn toward the negatively charged metal sites. The adsorbed molecules displace water on the metal surface, creating a protective barrier that prevents corrosion.[88] Through a chemisorption adsorption mechanism, SCS and GPP extract molecules can adsorb on the aluminum surface by transferring electrons between heteroatom electron pairs and empty p-orbitals of aluminum through donor–acceptor interactions. The molecules of SCS and GPP have a predicted value of ΔG^{0}_{ads} that is around 30 kJ mol^{-1}, signifying a comprehensive adsorption (physicochemical adsorption), but chemisorption main process between the inhibitor particles and the aluminum surface. These particles have formed a protective barrier that prevented the corrosive media from reaching the aluminum surface.

4.11. RSM results

Using *P*-values and *F*-values, ANOVA is a valuable tool for evaluating the relevance of models, individual experimental factors, and their interactions. Two models were established for the prediction of inhibition efficiency and corrosion rate based on the experimental results and ANOVA. Tables 15, 16, B13, and B14 (SI) represent the ANOVA outcomes with the Fit-statistics for the inhibition efficiency and corrosion rate models, both

Table 14 Data and specifications are obtained by simulating Monte Carlo to adsorb aluminum-SCS and GPP (neutral)

Plant	Compound	Total energy (kcal mol^{-1})	Adsorption energy (kcal mol^{-1})	Rigid adsorption energy (kcal mol^{-1})	Deformation energy (kcal mol^{-1})	Hydronium ion dE_{ad}/dN_i (kcal mol^{-1})	Water dE_{ad}/dN_i (kcal mol^{-1})	Chloride ion dE_{ad}/dN_i (kcal mol^{-1})	dE_{ad}/dN_i (kcal mol^{-1})
SCS&GPP	(+) Catechin	-4.423×10^3	-4.393×10^3	-4.566×10^3	172.769	−140.224	−7.687	−137.903	−60.142
SCS	Myricetin	-4.447×10^3	-4.407×10^3	-4.567×10^3	160.118	−150.812	−6.007	−144.756	−127.440
SCS&GPP	Quercetin	-4.414×10^3	-4.373×10^3	-4.534×10^3	161.381	−151.014	−8.196	−146.480	−59.797
SCS&GPP	Kaempferol	-4.450×10^3	-4.407×10^3	-4.563×10^3	155.861	−138.703	−1.020	−146.908	−58.715
SCS	Gallic acid	-4.410×10^3	-4.385×10^3	-4.557×10^3	172.320	−148.740	−6.384	−139.564	−49.870
SCS&GPP	*p*-OH-benzoic acid	-4.410×10^3	-4.385×10^3	-4.551×10^3	166.025	−156.158	−5.948	−141.132	−50.704
SCS&GPP	Protocatechuic acid	-4.449×10^3	-4.426×10^3	-4.596×10^3	170.214	−150.762	−7.629	−134.273	−63.440
SCS	Syringic acid	-4.392×10^3	-4.401×10^3	-4.568×10^3	167.595	−147.561	−5.737	−147.069	−60.053
SCS	Vanillic acid	-4.381×10^3	-4.372×10^3	-4.534×10^3	161.867	−143.767	−6.297	−143.653	−24.742
SCS	Chlorogenic acid	-4.395×10^3	-4.373×10^3	-4.522×10^3	149.747	−144.798	−5.661	−139.499	−60.342
SCS&GPP	Caffeic acid	-4.440×10^3	-4.356×10^3	-4.516×10^3	159.523	−146.120	−6.597	−143.301	−84.586
SCS	*p*-Coumaric acid	-4.491×10^3	-4.406×10^3	-4.576×10^3	169.688	−148.199	−1.688	−141.762	−16.493
SCS	Ferulic acid	-4.434×10^3	-4.369×10^3	-4.532×10^3	163.044	−148.880	−5.039	−126.622	−20.948
GPP	Naringenin	-4.43×10^3	-4.38×10^3	-4.55×10^3	169.986	−143.133	−6.179	−129.325	−106.491
GPP	Epigallocatechin	-4.49×10^3	-4.46×10^3	-4.63×10^3	171.353	−151.152	−8.488	−135.294	−132.634
GPP	Apigenin	-4.50×10^3	-4.43×10^3	-4.60×10^3	166.278	−153.676	−6.270	−134.245	−113.756
GPP	Melitidin	-4.48×10^3	-4.41×10^3	-4.57×10^3	157.118	−154.354	−6.007	−131.134	−106.459
GPP	Quinic acid	-4.39×10^3	-4.41×10^3	-4.58×10^3	166.168	−141.199	−9.033	−139.119	−88.094
GPP	2,2′-methylenebis	-4.46×10^3	-4.41×10^3	-4.57×10^3	159.061	−151.432	−8.406	−135.758	−83.952
GPP	Quercetin triglucoside	-4.41×10^3	-4.51×10^3	-4.65×10^3	144.464	−145.925	−7.494	−145.113	−173.287

Table 15 Analysis of variance and model summary for corrosion inhibition efficiency using SCS extract

Source	Sum of squares	df	Mean square	*F*-value	*p*-value	
Model	2184.89	9	242.77	14.49	0.0001	Significant
A – temperature	862.51	1	862.51	51.49	<0.0001	
B – Concentration	0.1959	1	0.1959	0.0117	0.9160	
C – time	303.78	1	303.78	18.13	0.0017	
AB	504.02	1	504.02	30.09	0.0003	
AC	0.0511	1	0.0511	0.0030	0.9571	
BC	226.55	1	226.55	13.52	0.0043	
A^2	12.12	1	12.12	0.7234	0.4149	
B^2	0.4960	1	0.4960	0.0296	0.8668	
C^2	53.15	1	53.15	3.17	0.1052	
Residual	167.52	10	16.75			
Lack of fit	167.52	4	41.88			
Pure error	0.0000	6	0.0000			
Cor total	2352.41	19				
Std. dev. 4.09	R^2 0.9288					
Mean 75.18	Adjusted R^2 0.8647					
C.V. % 5.44	Predicted R^2 −0.2415					
	Adeq precision 11.9727					

for SCS and GPP. The Swiss chard stem (SCS) extract analysis, using RSM, revealed that the inhibition efficiency was well described using a quadratic model, with a high explanatory power and satisfactory level of precision, temperature had a significant negative linear effect, and immersion time positively affected the inhibition efficiency, with significant interaction between temperature and concentration, and concentration and time, as supported by diagnostic plots of normality, close prediction and actual values in Fig. 20(a) and 21(a), and response surfaces in Fig. 22 showing efficiency maximum at high temperatures and maximum concentration. In the case of corrosion rate with SCS the model was found to be a good fit, with temperature and time accelerating kinetics and exposure dominating over concentration protective effect, with important interactions and quadratic effects showing nonlinear optima at intermediate conditions as demonstrated by diagnostics in Fig. 20(b) and 21(b), and surfaces in Fig. 23

Table 16 The adequacy and significance of the corrosion rate model were evaluated through an analysis of its fit statistics and ANOVA for SCS extract

Source	Sum of squares	df	Mean square	*F*-value	*p*-value	
Model	3.989×10^{-8}	9	4.432×10^{-9}	12.31	0.0003	Significant
A – temperature	2.025×10^{-8}	1	2.025×10^{-8}	56.24	<0.0001	
B – concentration	2.740×10^{-9}	1	2.740×10^{-9}	7.61	0.0202	
C – time	6.289×10^{-9}	1	6.289×10^{-9}	17.47	0.0019	
AB	1.875×10^{-9}	1	1.875×10^{-9}	5.21	0.0456	
AC	5.798×10^{-9}	1	5.798×10^{-9}	16.11	0.0025	
BC	6.423×10^{-10}	1	6.423×10^{-10}	1.78	0.2112	
A^2	6.929×10^{-9}	1	6.929×10^{-9}	19.25	0.0014	
B^2	5.152×10^{-10}	1	5.152×10^{-10}	1.43	0.2592	
C^2	2.128×10^{-9}	1	2.128×10^{-9}	5.91	0.0354	
Residual	3.600×10^{-9}	10	3.600×10^{-10}			
Lack of fit	1.178×10^{-9}	4	2.944×10^{-10}	0.7294	0.6035	Not significant
Pure error	2.422×10^{-9}	6	4.037×10^{-10}			
Cor total	4.349×10^{-8}	19				
Std. dev. 0.0000	R^2 0.9172					
Mean 0.0000	Adjusted R^2 0.8427					
C.V. % 69.16	Predicted R^2 0.4471					
	Adeq precision 14.1313					

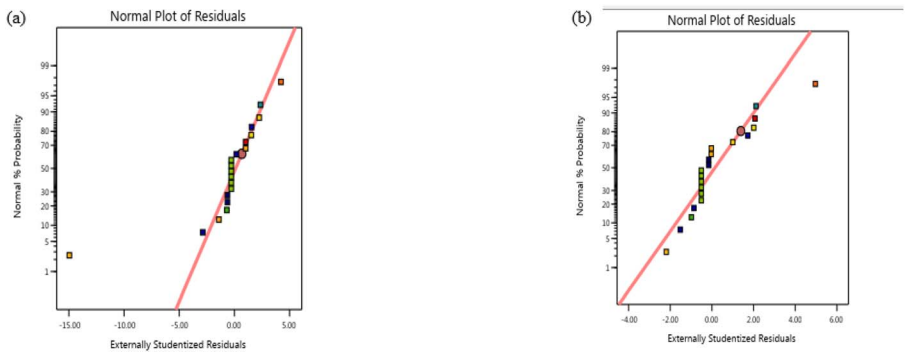

Fig. 20 The normal probability plots for the externally studentized residuals of the corrosion inhibition efficiency (CIE) (a) and corrosion rate (CR) model (b) of SCS extract.

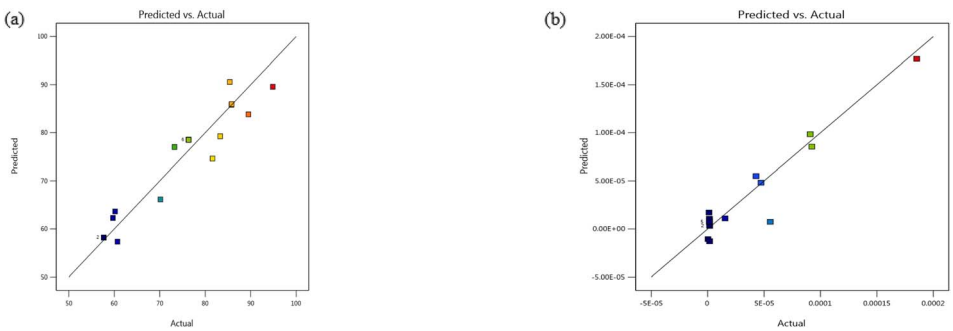

Fig. 21 Plot of predicted *versus* actual values for the (a) inhibition efficiency model and (b) corrosion rate model of SCS extract.

showing minima at low temperatures and moderate times/concentrations.

The same procedure was performed on green pea peel (GPP) extract, as shown in Fig. A6–A9 (SI). In comparison of the two plants, SCS tends to be more effective in inhibition than GPP, due to its more diverse range of phenolic compounds, such as syringic acid and kaempferol, which are probably easier to form stable protective coats on aluminum surfaces, so the models of their interaction are more complicated, but GPP, with its more abundant flavonoids such as catechin and epicatechin, exhibit simpler, linear-dominant dynamics, being more affected by temperature changes.

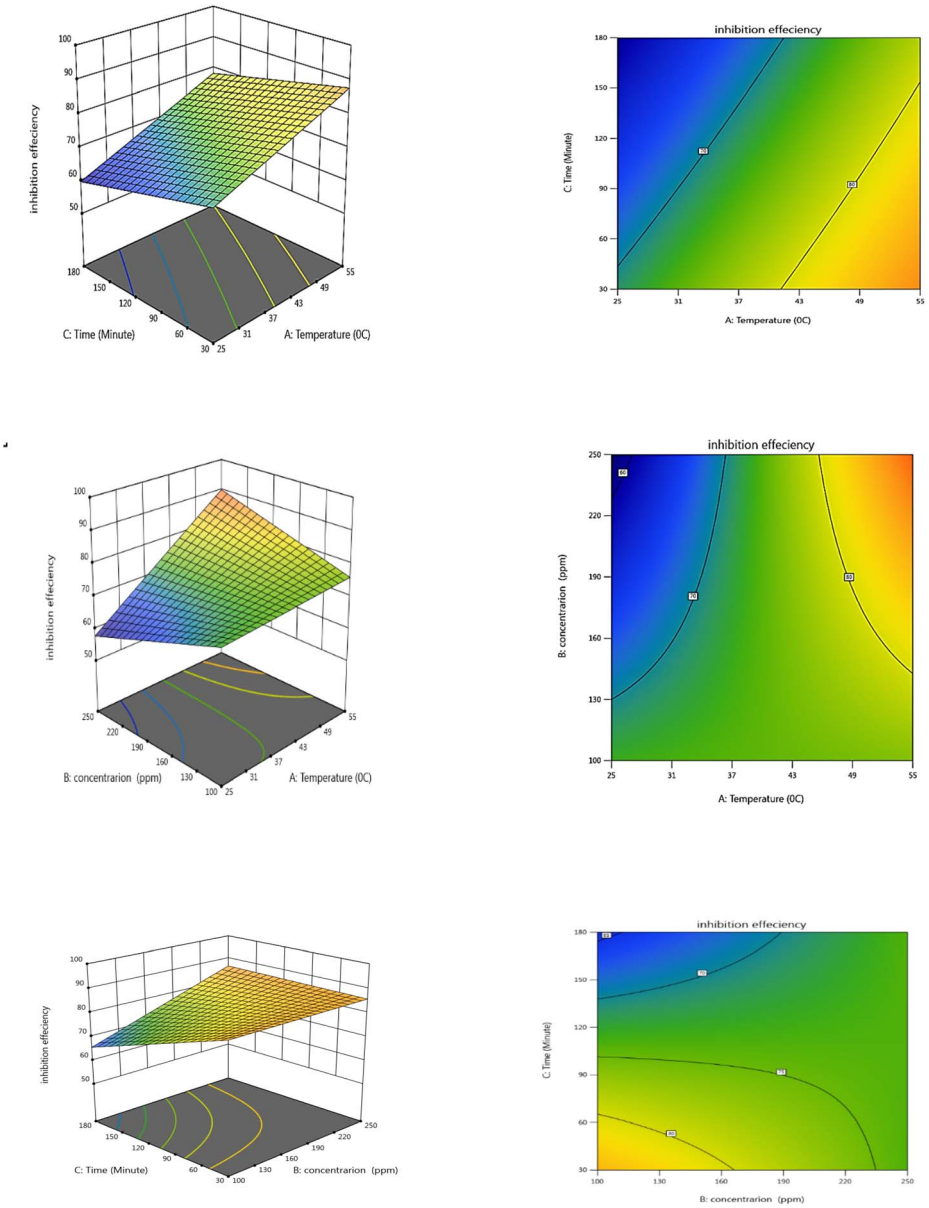

Fig. 22 Interaction of variables' effects on the effectiveness of inhibition of SCS extract.

Comparing the two plants, SCS exhibits a better inhibition ability than GPP on average, due to its more diverse range of phenolic compounds such as syringic acid and kaempferol, which probably produce more stable protective films on the aluminum surfaces, leading to more complex interactions in the models, whereas GPP, with flavonoids including catechin and epicatechin, displays only simple and linear-dominant behaviour, as a consequence of highly effective physisorption and strong sensitivity to temperature changes.

These RSM results agree qualitatively with the results, in which weight loss measurements revealed effectiveness increases with concentration and moderate temperatures, electrochemical measurements revealed mixed-type inhibitory actions with polarization curve shifts, surface characterization measurements using XPS and AFM revealed the formation of protective layers that reduced roughness, and adsorption measurements favored the Langmuir isotherm to the Henry isotherm, as did thermodynamic parameters indicating endothermic processes and spontaneous adsorption, which are consistent with quadratic curvatures and optima in the models, and quantum chemical and molecular dynamics simulations supported.

Recent studies strengthen these patterns in green corrosion inhibition for aluminum in acidic media; for instance, *Euphorbia neriifolia* extracts demonstrated effective inhibition through similar concentration-dependent protection and temperature sensitivities in HCl environments.[89] *Ajuga orientalis* L. extract was evaluated as a sustainable inhibitor, showing enhanced efficiency *via* phenolic adsorption in HCl solutions, aligning with SCS's superior phenolic-driven

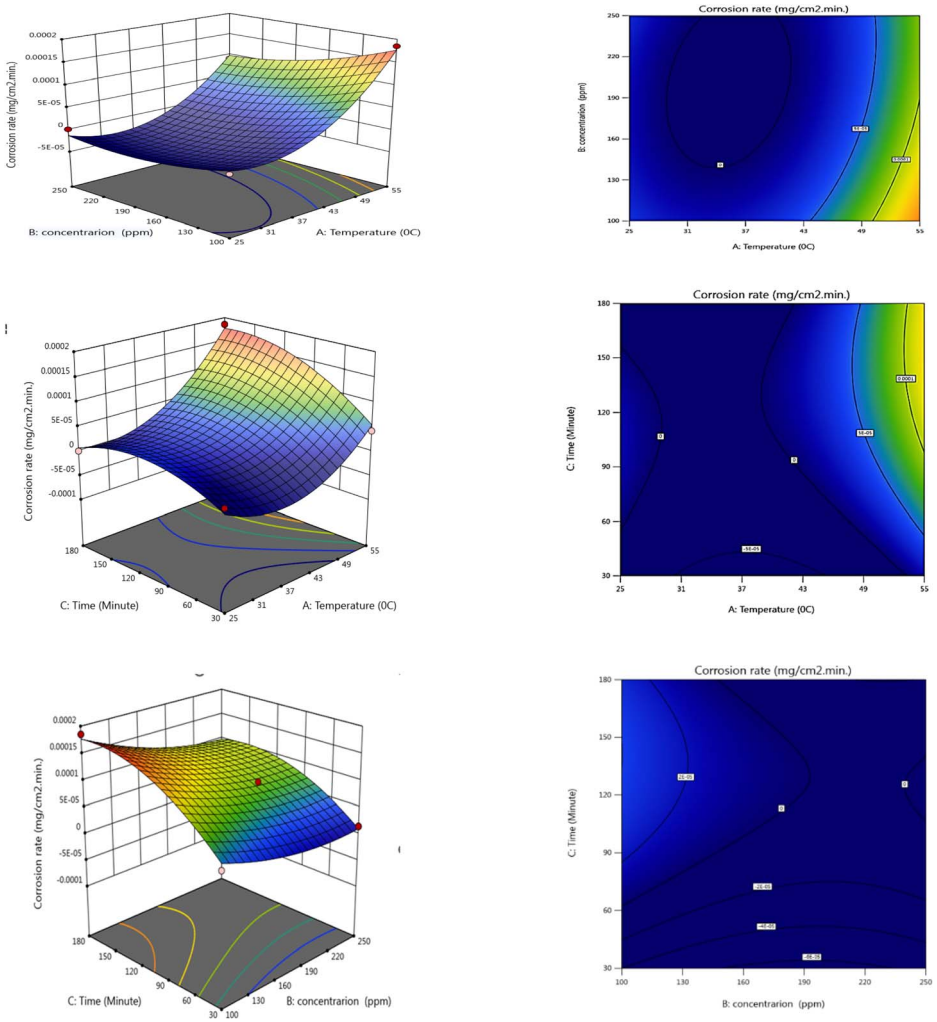

Fig. 23 Interaction of variables' effects on the rate of corrosion after using SCS extract.

performance.[90] Hibiscus sabdariffa leaf extract mitigated aluminum corrosion in varying HCl concentrations, emphasizing plant-based inhibitors' eco-friendly potential and concentration–time interactions akin to those in RSM models.[29] *Araucaria heterophylla* served as a green inhibitor for mild steel in acidic cleaning, highlighting thermodynamic spontaneity and film formation comparable to the study's observations.[91] A comprehensive review on phytochemicals as inhibitors for mild steel and aluminum in corrosive settings underscored the role of active plant ingredients in achieving high protection, supporting the comparative advantages of SCS over GPP.[92]

4.12. Studies on comparative economics

Green corrosion inhibitors found in fruit seeds, leaves, roots, and shells have gained a lot of interest as a possible replacement for other harmful inhibitors. The existence of active functional groups and one or more heteroatoms within the organic compound results in a high inhibitory efficiency. In this study, 91.5 and 83.1 percent efficiencies were achieved based on the weight loss tests of using 250 ppm extract of Swiss chard

Table 17 Concise cost estimation of the extraction processes of SCS and GPP

Cost of 1 kg raw Pisum		$0.6	
Cost of 1 L pure methanol		$1.4	
Cost of 1 kg Pisum nuts		$1.4	
To extract 1 kg from GPP			
Raw Pisum needed	138.88 kg	Cost	$83.33
Pisum nuts	55.55 kg	Cost	$77.77
Pisum peels	83.33 kg	Cost	$5.55
Methanol needed	29.16 L	Cost	$40.83
Cost of 1 kg from GPP extract		$46.38	
Cost of 1 kg raw Swiss chard		$0.7	
Cost of 1 L pure methanol		$1.4	
Cost of 1 kg Swiss chard leaves		$1.1	
To extract 1 kg from SCS			
Raw Swiss chard needed	148.14 kg	Cost	$103.70
Swiss chard leaves	81.48 kg	Cost	$89.62
Swiss chard stems	66.66 kg	Cost	$14.07
Methanol needed	20 L	Cost	$28
Cost of 1 kg from SCS extract		$42.07	

stems and green pea pods, respectively. The expense of creating 1 kg of Swiss chard stem extract is found to be around $42, while around $46 is the expense of creating 1 kg of green pea pod extract, as included in Table 17. The majority of the extraction processes of green inhibitors cost more than $50 per kg.[58]

5. Conclusion

The extracts of Swiss chard stem (SCS) and green pea peel (GPP) demonstrated good inhibitory behavior against the corrosion of pure aluminum surfaces in aggressive media of 1 M HCl. Electrochemical studies (electrochemical impedance spectroscopy, potentiodynamic polarization), weight loss (WL), molecular dynamics (MD) simulations, quantum chemical calculations, and surface examination by AFM and XPS were employed to evaluate the impact of the corrosion inhibition of SCS and GPP extracts. The inhibition efficiency of SCS and GPP extracts increases upon an increase in concentration and an elevated temperature. The % I.E. of SCS and GPP extracts were found to be 91.5% and 83.1%, respectively, using the gravimetric method. Tafel plots indicated a mixed type of inhibition of both extract molecules. A reduction in double-layer capacitances was observed due to increased inhibitor' doses. The adsorption of SCS and GPP extract molecules over the Al surface obeyed mainly the Langmuir adsorption model rather than the Henry model. The molecules of the extracts were adsorbed to the Al chemically. According to surface examinations, the extracts adsorbed to the aluminum surface, forming a layer that inhibited the dissolution of the metal. The experimental data derived from the mass loss technique and the electrochemical methods were all in agreement. Further, AFM and XPS analyses also validate the data obtained from the WL and the electrochemical techniques. The adsorption of certain extract constituents over the Al (111) surface was simulated using molecular dynamics, which showed strong interactions. Theoretical calculations and practical results showed that SCS and GPP extracts possess the potential to expand as eco-friendly inhibitors.

Conflicts of interest

The authors declare that they have no known competing financial interests or personal relationships that could have appeared to influence the work reported in this paper.

Data availability

The supplementary information (SI) and the article provide the data that support the study's conclusions. Supplementary information: Fig. A1: WL of Al in 1 M HCl with and without different specific concentrations of SCS extract for various submerge periods at various temperatures; Fig. A2: WL of Al in 1 M HCl with and without different specific concentrations of GPP extract for various submerge periods at various temperatures; Fig. A3: Plots of studied isotherms of Swiss chard stem extract for corrosion of aluminum in 1 M HCl, at different temperatures using WL method; Fig. A4: Plots of studied isotherms of green pea peels extract for corrosion of aluminum in 1 M HCl, at different temperatures applying WL method; Fig. A5: A graphic depiction of SCS and GPP compounds' Fukui indices for their more reactive atoms in both their protonated and non-protonated systems; Fig. A6: The normal probability plots for the externally studentized residuals of the corrosion inhibition efficiency (CIE) and corrosion rate (CR) models of GPP extract; Fig. A7: Plot of predicted versus actual values for the (a) inhibition efficiency model and (b) corrosion rate model of GPP extract; Fig. A8: Interaction of variables' effects on the effectiveness of inhibition of GPP extract; Fig. A9: Interaction of variables' effects on the rate of corrosion after using GPP extract; Table B1: The important components of SCS extract; Table B2: The important components of GPP extract; Table B3: Correlation coefficient (R^2) for different adsorption isotherms for adsorption of SCS extract on the Al surface at different temperatures after 90 minutes' immersion time; Table B4: Correlation coefficient (R^2) for different adsorption isotherms for adsorption of GPP extract on the Al surface at different temperatures after 90 minutes' immersion time; Table B5: The HOMO and LUMO orbital distribution and molecular structure optimization for important components in SCS and GPP extracts were determined *via* the DMol^3/GGA/BOP approach (protonated); Table B6: The quantum data for Swiss chard stems extract in the neutral, protonated, and vacuum form; Table B7: The quantum data for green pea peel extract in the neutral, protonated, and vacuum form; Table B8: Calculated Mullikan charge on the atoms of the investigated neutral, protonated, and vacuum inhibitor molecules of SCS and GPP; Table B9: The electrostatic potentials of the neutral and protonated molecules as the contour of the SCS and GPP extracts' electrostatic field; Table B10: The best formation for adsorption of SCS and GPP extracts on aluminum (1 1 1) substrate as determined by the adsorption locator module; Table B11: Data and specifications are obtained by simulating Monte Carlo to adsorb aluminum-SCS and GPP (protonated); Table B12: Data and specifications are obtained by simulating Monte Carlo to adsorb aluminum-SCS and GPP (vacuum form); Table B13: Analysis of variance and model summary for corrosion inhibition efficiency using GPP extract; Table B14: The adequacy and significance of the corrosion rate model were evaluated through an analysis of its fit statistics and ANOVA for GPP extract. See DOI: https://doi.org/10.1039/d5ra09501h.

References

1 S. A. Umoren, M. M. Solomon, I. B. Obot and R. K. Suleiman, A critical review on the recent studies on plant biomaterials as corrosion inhibitors for industrial metals, *J. Ind. Eng. Chem.*, 2019, **76**, 91–115, DOI: 10.1016/j.jiec.2019.03.057.
2 M. Sahraoui, M. Boulkroune, A. Chibani, Y. Larbah and A. Abdessemed, Aqueous Extract of Punica Granatum Fruit Peel as an Eco-Friendly Corrosion Inhibitor for Aluminium Alloy in Acidic Medium, *J. Bio-Tribo.-Corrosion*, 2022, **8**(2), 1–10, DOI: 10.1007/s40735-022-00658-0.
3 M. Prabakaran, S. H. Kim, A. Sasireka, K. Kalaiselvi and I. M. Chung, Polygonatum odaratum extract as an eco-

friendly inhibitor for aluminum corrosion in acidic medium, *J. Adhes. Sci. Technol.*, 2018, **32**(18), 2054–2069, DOI: 10.1080/01694243.2018.1462947.

4 A. Ennouri, A. Lamiri and M. Essahli, Corrosion inhibition of aluminium in acidic media by different extracts of Trigonellafoenum-graecum L seeds, *Port. Electrochim. Acta*, 2017, **35**(5), 279–295, DOI: 10.4152/pea.201705279.

5 J. Haque, M. A. Zulaikha, W. B. W. Nik, W. Daoudi, E. Berdimurodov and F. Zulkifli, Alocasia Odora Extract as Environmentally Benign Corrosion Inhibitor for Aluminum in HCl, *Moroccan J. Chem.*, 2023, **11**(4), 1013–1026, DOI: 10.48317/IMIST.PRSM/morjchem-v11i04.41618.

6 K. Krishnaveni and J. Ravichandran, Aqueous extract of leaves of Morinda tinctoria as a corrosion inhibitor for aluminum in sulphuric acid medium, *J. Adhes. Sci. Technol.*, 2015, **29**(14), 1465–1482, DOI: 10.1080/01694243.2015.1030907.

7 I. Y. Suleiman, M. Abdulwahab and M. Z. Sirajo, Anti-corrosion Properties of Ethanol Extract of Acacia senegalensis stem on Al–Si–Fe/SiC Composite in Sulfuric Acid Medium, *J. Fail. Anal. Prev.*, 2018, **18**(1), 212–220, DOI: 10.1007/s11668-018-0399-3.

8 U. L. Ezeamaku, C. B. Ezekannagha, O. I. Eze, I. C. Onyechere and O. D. Onukwuli, Corrosion Inhibition of Aluminum using Guava Leaf Extract as an Inhibitor, *Moroccan J. Chem.*, 2023, **11**(3), 763–779, DOI: 10.48317/IMIST.PRSM/morjchem-v11i3.40322.

9 M. Abdallah, A. Al-Rashidi, N. El Guesmi, A. S. Al-Gorair and S. S. Al-Juaid, Insights into corrosion inhibition of aluminum in hydrochloric acid solutions using expired cephalosporins and klavox: Chemical, electrochemical and theoretical approaches, *Int. J. Electrochem. Sci.*, 2024, **19**(9), 100741, DOI: 10.1016/j.ijoes.2024.100741.

10 K. G. Prajapati, P. S. Desai, B. B. Parmar and A. M. Patel, Comprehensive study on the corrosion inhibition of aluminum in HCl by N1, N1'-(ethane-1,2-diyl)di(ethane-1,2-diamine): Experimental and theoretical approaches, *Results Surf. Interfaces*, 2024, **17**, 100347, DOI: 10.1016/j.rsurfi.2024.100347.

11 J. Halambek, A. Žutinić and K. Berković, Ocimum basilicum L. oil as corrosion inhibitor for aluminium in hydrochloric acid solution, *Int. J. Electrochem. Sci.*, 2013, **8**(9), 11201–11214, DOI: 10.1016/s1452-3981(23)13180-4.

12 N. Raghavendra and J. Ishwara Bhat, Green approach to inhibition of corrosion of aluminum in 0.5 M HCl medium by tender arecanut seed extract: insight from gravimetric and electrochemical studies, *Res. Chem. Intermed.*, 2016, **42**(7), 6351–6372, DOI: 10.1007/s11164-016-2467-1.

13 M. E. Eissa, S. H. Etaiw, E. S. El-Hussieny, A. A. El-Hossiany and A. E. A. S. Fouda, Sweet Orange Peel Extract as green sustainable corrosion inhibitor for Al in 1 M HCl, *Int. J. Electrochem. Sci.*, 2025, **20**(1), 100882, DOI: 10.1016/j.ijoes.2024.100882.

14 O. U. Abakedi and J. E. Asuquo, Corrosion Inhibition of Aluminium in Acidic Medium by Ethanol Leaf Extract of Azadirachta Indica, *J. Basic Appl. Res.*, 2016, **2**(4), 556–560.

15 N. B. Iroha and N. J. Maduelosi, Corrosion inhibitive action and adsorption behaviour of justicia secunda leaves extract as an eco-friendly inhibitor for aluminium in acidic media, *Biointerface Res. Appl. Chem.*, 2021, **11**(5), 13019–13030, DOI: 10.33263/BRIAC115.1301913030.

16 A. S. Fouda, S. M. Rashwan, M. M. Kamel and E. A. Haleem, Inhibitive Influence of Cumin (Cuminum Cyminum) Seed Extract on the Dissolution of Al in 2 M HCl Acid Medium, *J. Bio- Tribo.-Corrosion*, 2021, **7**(2), 1–14, DOI: 10.1007/s40735-021-00480-0.

17 R. D. Alghamdi, L. S. Alqarni, M. D. Alghamdi, N. F. Alotaibi and H. Gadow, Experimental and Theoretical Investigations on the Use of Pumpkin Peel as a Sustainable Biomass Anticorrosion Agent for Aluminum in HCl Solutions, *J. Chem.*, 2024, **2024**, 1–26, DOI: 10.1155/2024/5696212.

18 A. K. Maayta and N. A. F. Al-Rawashdeh, Inhibition of acidic corrosion of pure aluminum by some organic compounds, *Corros. Sci.*, 2004, **46**(5), 1129–1140, DOI: 10.1016/j.corsci.2003.09.009.

19 G. Nasir, S. Zaidi, N. Tabassum and Asfaq, A review on nutritional composition, health benefits and potential applications of by-products from pea processing, *Biomass Convers. Biorefinery*, 2024, **14**(10), 10829–10842, DOI: 10.1007/s13399-022-03324-0.

20 N. Čeryová *et al.*, Nutritional Composition , Polyphenol Content , and Antioxidant Activity of Swiss Chard (Beta vulgaris L. subsp. cicla, *Agrobiodiversity for Improving Nutrition Health and Life Quality*, 2025, vol. 2025, pp. 128–135.

21 Y. H. Pyo, T. C. Lee, L. Logendra and R. T. Rosen, Antioxidant activity and phenolic compounds of Swiss chard (Beta vulgaris subspecies cycla) extracts, *Food Chem.*, 2004, **85**(1), 19–26, DOI: 10.1016/S0308-8146(03)00294-2.

22 F. Guo, *et al.*, Phenolics of Green Pea (Pisum sativum L.) Hulls, Their Plasma and Urinary Metabolites, Bioavailability, and in Vivo Antioxidant Activities in a Rat Model, *J. Agric. Food Chem.*, 2019, **67**(43), DOI: 10.1021/acs.jafc.9b04501.

23 N. S. Abdelshafi, M. A. Sadik, M. A. Shoeib and S. Abdel, Corrosion inhibition of aluminum in 1 M HCl by novel pyrimidine derivatives , EFM measurements , DFT calculations and MD simulation, *Arab. J. Chem.*, 2022, **15**(1), 103459, DOI: 10.1016/j.arabjc.2021.103459.

24 M. M. El-Deeb, S. M. Sayyah, S. S. Abd El-Rehim and S. M. Mohamed, Corrosion inhibition of aluminum with a series of aniline monomeric surfactants and their analog polymers in 0.5M HCl solution. Part II: 3-(12-sodiumsulfonate dodecyloxy) aniline and its analog polymer, *Arab. J. Chem.*, 2015, **8**(4), 527–537, DOI: 10.1016/j.arabjc.2013.09.018.

25 A. Toghan, H. S. Gadow, H. M. Dardeer and H. M. Elabbasy, New promising halogenated cyclic imides derivatives as potential corrosion inhibitors for carbon steel in hydrochloric acid solution, *J. Mol. Liq.*, 2021, **325**, 115136, DOI: 10.1016/j.molliq.2020.115136.

26 A. Toghan, H. S. Gadow, A. Fawzy, H. Alhussain and H. Salah, Adsorption Mechanism, Kinetics,

Thermodynamics, and Anticorrosion Performance of a New Thiophene Derivative for C-Steel in a 1.0 M HCl: Experimental and Computational Approaches, *Metals*, 2023, **13**(9), 1–22, DOI: 10.3390/met13091565.

27 H. S. Gadow, T. A. Farghaly and A. M. Eldesoky, In an Acidic Environment, Perimidin-10-one Derivatives were Evaluated as Potential Copper Corrosion Inhibitors (Experimental and Theoretical Examinations), *J. Bio.-Tribo.-Corrosion*, 2022, **8**(2), 1–32, DOI: 10.1007/s40735-022-00650-8.

28 H. M. Elabbasy, A. Toghan and H. S. Gadow, Cysteine as an Eco-Friendly Anticorrosion Inhibitor for Mild Steel in Various Acidic Solutions: Electrochemical, Adsorption, Surface Analysis, and Quantum Chemical Calculations, *ACS Omega*, 2023, **9**, 13391–13411, DOI: 10.1021/acsomega.3c10522.

29 J. C. Emereole and A. I. Ikeuba, Response surface methodology and experimental evaluation of the inhibitory properties of corn leaf extract for aluminum corrosion in acid media, *Anti-Corrosion Methods and Materials*, 2025, **71**(6), 593–605, DOI: 10.1108/ACMM-03-2024-2988.

30 M. Olfatmiri, M. B. Gholivand, M. Mahdavian and A. Mahmoudi Nahavandi, Adiantum Capillus-Veneris Extract as a Sustainable Inhibitor to Mitigate Corrosion in Acid Solutions: Experimental, Machine-Learning Simulation, and Multiobjective Optimization, *Langmuir*, 2024, **40**(50), 26396–26411, DOI: 10.1021/ACS.LANGMUIR.4C02659.

31 A. Zakeri, E. Bahmani and A. S. R. Aghdam, Plant extracts as sustainable and green corrosion inhibitors for protection of ferrous metals in corrosive media: A mini review, *Corros. Commun.*, 2022, **5**, 25–38, DOI: 10.1016/j.corcom.2022.03.002.

32 N. O. Eddy, P. O. Ameh and O. Odiongenyi, Physicochemical Characterization and Corrosion Inhibition Potential of Ficus Benjamina (FB) Gum, *Walailak Journal of Science and Technology*, 2014, **32**(3), 183–197, DOI: 10.4152/pea.201403183.

33 L. Larabi, Y. Harek, O. Benali and S. Ghalem, Hydrazide derivatives as corrosion inhibitors for mild steel in 1 M HCl, *Progress in Organic Coatings*, 2005, **54**, 256–262, DOI: 10.1016/j.porgcoat.2005.06.015.

34 N. O. Eddy, U. J. Ibok, P. O. Ameh, N. O. Alobi and M. M. Sambo, Adsorption and quantum chemical studies on the inhibition of the corrosion of aluminum in hcl by gloriosa superba (GS) gum, *Chem. Eng. Commun.*, 2014, **201**(10), 1360–1383, DOI: 10.1080/00986445.2013.809000.

35 E. Khamis, A. M. Abdel-Gaber, M. Morshidy and M. E. Mohamed, Eco-friendly inhibitors for sustainable corrosion protection of mild steel under oilfield acidizing conditions, *Sci. Rep.*, 2025, **15**(1), 1–19, DOI: 10.1038/s41598-025-27271-8.

36 K. Xhanari and M. Finšgar, Organic corrosion inhibitors for aluminum and its alloys in chloride and alkaline solutions: A review, *Arab. J. Chem.*, 2019, **12**(8), 4646–4663, DOI: 10.1016/j.arabjc.2016.08.009.

37 H. M. Hassan, Electrochemical and computational investigation of Cicer arietinum extract as renewable and environmentally green corrosion inhibitor for aluminium in acidic environment, *Sci. Rep.*, 2025, **15**(1), 1–22, DOI: 10.1038/s41598-025-96141-0.

38 N. K. Shah, D. G. Ladha, P. M. Wadhwani, S. Thakur, M. Lone and P. C. Jha, Corrosion inhibition performance of Coriander Seeds extract molecules for pure Aluminum in Hydrochloric acid Medium: A combined Experimental and Quantum chemical approach, *Res. J. Recent Sci.*, 2016, **5**(1), 27–34.

39 F. M. Abu Orabi, *et al.*, Ajuga orientalis L. Extract as a Green Corrosion Inhibitor of Aluminum in an Acidic Solution: An Experimental and DFT Study, *Metals*, 2024, **14**(11), 1227–1247, DOI: 10.3390/met14111227.

40 J. Halambek and M. Gojo, *Inhibition of Acidic Aluminium Corrosion Using Ethanot Solution*, 2014.

41 M. Akin, S. Nalbantoglu, O. Cuhadar, D. Uzun and N. Saki, Juglans regia L. extract as green inhibitor for stainless steel and aluminium in acidic media, *Res. Chem. Intermed.*, 2015, **41**(2), 899–912, DOI: 10.1007/s11164-013-1241-x.

42 K. Shalabi, A. S. Fouda, G. Y. Elewady and A. El-Askalany, Adsorption and inhibitive properties of Phoenix dactylifera L. Extract as a green inhibitor for aluminum and aluminum-silicon alloy in HCl, *Prot. Met. Phys. Chem. Surfaces*, 2014, **50**(3), 420–431, DOI: 10.1134/S2070205114030174.

43 M. Radi, *et al.*, Pumpkin seeds as an eco-friendly corrosion inhibitor for 7075-T6 alloy in 3.5% NaCl solution: Electrochemical, surface and computational studies, *J. Mol. Liq.*, 2021, **337**, 116547, DOI: 10.1016/j.molliq.2021.116547.

44 N. Zulfareen, K. Kannan, T. Venugopal and S. Gnanavel, Synthesis, characterization and corrosion inhibition efficiency of N-(4-(Morpholinomethyl Carbamoyl Phenyl) Furan-2-Carboxamide for brass in HCl medium, *Arab. J. Chem.*, 2016, **9**(1), 121–135, DOI: 10.1016/j.arabjc.2015.08.023.

45 E. E. Oguzie, V. O. Njoku, C. K. Enenebeaku, C. O. Akalezi and C. Obi, Effect of hexamethylpararosaniline chloride (crystal violet) on mild steel corrosion in acidic media, *Corros. Sci.*, 2008, **50**(12), 3480–3486, DOI: 10.1016/j.corsci.2008.09.017.

46 P. O. Ameh and N. O. Eddy, Commiphora pedunculata gum as a green inhibitor for the corrosion of aluminium alloy in 0.1 M HCl, *Res. Chem. Intermed.*, 2014, **40**(8), 2641–2649, DOI: 10.1007/s11164-013-1117-0.

47 vizhi. I. Malar, S. Selvaraj and K. Kalirajan, Corrosion Behavior Of Mild Steel In Nattural Sea Water With TephrosiaPurpurea– A Green Approach, *Int. J. Res. Anal. Rev.*, 2018, **5**(4), 164–174.

48 L. Herrag, *et al.*, Adsorption properties and inhibition of mild steel corrosion in hydrochloric solution by some newly synthesized diamine derivatives: Experimental and theoretical investigations, *Corros. Sci.*, 2010, **52**(9), 3042–3051, DOI: 10.1016/j.corsci.2010.05.024.

49 Y. Sangeetha, S. Meenakshi and C. S. Sundaram, Interactions at the mild steel acid solution interface in the presence of O-fumaryl-chitosan: Electrochemical and

surface studies, *Carbohydr. Polym.*, 2016, **136**, 38–45, DOI: 10.1016/j.carbpol.2015.08.057.

50 A. Hamdy and N. S. El-Gendy, Thermodynamic, adsorption and electrochemical studies for corrosion inhibition of carbon steel by henna extract in acid medium, *Egypt. J. Pet.*, 2013, **22**(1), 17–25, DOI: 10.1016/j.ejpe.2012.06.002.

51 S. Hadisaputra, A. A. Purwoko, A. Hakim, R. Wati, D. Asnawati and Y. P. Prananto, Experimental and Theoretical Study of Pinostrobin as Copper Corrosion Inhibitor at 1 M H2SO4 Medium, *IOP Conf. Ser. Mater. Sci. Eng.*, 2020, **833**(1), 1–8, DOI: 10.1088/1757-899X/833/1/012010.

52 O. E.F, Corrosion Inhibition Behaviour for Mild Steel by Extracts of Musa sapientum Peels in HCl Solution: Kinetics and Thermodynamics Study, *IOSR J. Appl. Chem.*, 2012, **2**(6), 15–23, DOI: 10.9790/5736-0261523.

53 I. M. Vizhi, *Adsorption and Electrochemical Behavior of Cyperus Rotundus on Oil and Gas pipeline Steel in 1.0N Hydrochloric Acid*, 2023.

54 N. Arrousse, *et al.*, Fluorescein as commercial and environmentally friendly inhibitor against corrosion of mild steel in molar hydrochloric acid medium, *Mater. Today Proc.*, 2020, **27**, 3184–3192, DOI: 10.1016/j.matpr.2020.04.201.

55 F. Mohamed BinYehmed and R. Peel, Green Corrosion Inhibitor of Aluminum in Artificial Acid Rain by Rambutan Peel Extract, *Jopas*, 2019, **18**(4), 528–533.

56 M. Yadav, U. Sharma and P. Yadav, Corrosion inhibitive properties of some new isatin derivatives on corrosion of N80 steel in 15% HCl, *Int. J. Ind. Chem.*, 2013, **4**(1), 1–10, DOI: 10.1186/2228-5547-4-6.

57 H. Fathima, M. Pais and P. Rao, Anticorrosion performance of biopolymer pectin on 6061 aluminium alloy: Electrochemical, spectral and theoretical approach, *J. Mol. Struct.*, 2021, **1243**, 130775, DOI: 10.1016/j.molstruc.2021.130775.

58 H. S. Gadow and M. Fakeeh, Green inhibitor of carbon steel corrosion in 1 M hydrochloric acid: Eruca sativa seed extract (experimental and theoretical studies), *RSC Adv.*, 2022, **12**(15), 8953–8986, DOI: 10.1039/d2ra01296k.

59 M. M. Solomon, H. Gerengi and S. A. Umoren, Carboxymethyl Cellulose/Silver Nanoparticles Composite: Synthesis, Characterization and Application as a Benign Corrosion Inhibitor for St37 Steel in 15% H2SO4 Medium, *ACS Appl. Mater. Interfaces*, 2017, **9**(7), 6376–6389, DOI: 10.1021/acsami.6b14153.

60 N. M. El-Basiony, *et al.*, Theoretical and experimental insights into the C-steel aqueous corrosion inhibition at elevated temperatures in 1.0M HCl via multi-carbonyl Gemini cationic surfactants, *Zeitschrift fur Phys. Chemie*, 2023, **237**(6), 707–736, DOI: 10.1515/zpch-2023-0219.

61 N. Raghavendra and J. I. Bhat, Natural Products for Material Protection: An Interesting and Efficacious Anticorrosive Property of Dry Arecanut Seed Extract at Electrode (Aluminum)–Electrolyte (Hydrochloric Acid) Interface, *J. Bio- Tribo-Corrosion*, 2016, **2**(4), 1–14, DOI: 10.1007/s40735-016-0051-2.

62 R. S. Abdel Hameed, E. A. Ismail, A. H. Abu-Nawwas and H. I. Al-Shafey, Expired voltaren drugs as corrosion inhibitor for aluminium in hydrochloric acid, *Int. J. Electrochem. Sci.*, 2015, **10**(3), 2098–2109, DOI: 10.1016/s1452-3981(23)04832-0.

63 C. Kamal and M. G. Sethuraman, Caulerpin-A bis-indole alkaloid as a green inhibitor for the corrosion of mild steel in 1 M HCl solution from the marine alga caulerpa racemosa, *Ind. Eng. Chem. Res.*, 2012, **51**(31), 10399–10407, DOI: 10.1021/ie3010379.

64 H. M. Elabbasy and H. S. Gadow, Study the effect of expired tenoxicam on the inhibition of carbon steel corrosion in a solution of hydrochloric acid, *J. Mol. Liq.*, 2021, **321**, 114918, DOI: 10.1016/j.molliq.2020.114918.

65 E. E. El-Katori, A. S. Fouda and R. R. Mohamed, Synergistic corrosion inhibition activity of the chicoriumintybus extract and iodide ions for mild steel in acidic media, *J. Chil. Chem. Soc.*, 2020, **65**(1), 4672–4681, DOI: 10.4067/S0717-97072020000104672.

66 M. Outirite, *et al.*, ac impedance, X-ray photoelectron spectroscopy and density functional theory studies of 3,5-bis(n-pyridyl)-1,2,4-oxadiazoles as efficient corrosion inhibitors for carbon steel surface in hydrochloric acid solution, *Electrochim. Acta*, 2010, **55**(5), 1670–1681, DOI: 10.1016/j.electacta.2009.10.048.

67 H. S. Gadow, T. A. Farghaly and A. M. Eldesoky, Experimental and theoretical investigations for some spiropyrazoles derivatives as corrosion inhibitors for copper in 2 M HNO3 solutions, *J. Mol. Liq.*, 2019, **294**, 111614, DOI: 10.1016/j.molliq.2019.111614.

68 A. A. Farag, A. S. Ismail and M. A. Migahed, Squid By-product Gelatin Polymer as an Eco-friendly Corrosion Inhibitor for Carbon Steel in 0.5 M H2SO4 Solution: Experimental, Theoretical, and Monte Carlo Simulation Studies, *J. Bio-Tribo-Corrosion*, 2020, **6**(1), 1–15, DOI: 10.1007/s40735-019-0310-0.

69 R. D. Alghamdi, M. D. Alghamdi and H. S. Gadow, Use of expired Sulbutiamine drug as anticorrosive agent for carbon steel in hydrochloric acid solution, *Int. J. Corros. Scale Inhib.*, 2023, **12**(4), 2282–2326, DOI: 10.17675/2305-6894-2023-12-4-45.

70 M. I. El-tantawy, H. S. Gadow, I. G. Rashed and A. E. S. Fouda, Inhibition of Copper Corrosion by Rice Straw Extract in 2M Solution of Nitric Acid, *Biointerface Res. Appl. Chem.*, 2021, **12**(1), 83–104, DOI: 10.33263/briac121.083104.

71 M. A. Migahed, A. A. Farag, S. M. Elsaed, R. Kamal, M. Mostfa and H. A. El-Bary, Synthesis of a new family of Schiff base nonionic surfactants and evaluation of their corrosion inhibition effect on X-65 type tubing steel in deep oil wells formation water, *Mater. Chem. Phys.*, 2011, **125**(1–2), 125–135, DOI: 10.1016/j.matchemphys.2010.08.082.

72 B. R. Holla, R. Mahesh, H. R. Manjunath and V. R. Anjanapura, Plant extracts as green corrosion inhibitors for different kinds of steel: A review, *Heliyon*, 2024, **10**(14), 1–20, DOI: 10.1016/j.heliyon.2024.e33748.

73 H. Lin, *et al.*, Corrosion Inhibition Properties of Corrosion Inhibitors to under-Deposit Corrosion of X65 Steel in CO2 Corrosion Conditions, *Molecules*, 2024, **29**(11), 1–18, DOI: 10.3390/molecules29112611.

74 P. Singh, V. Srivastava and M. A. Quraishi, Novel quinoline derivatives as green corrosion inhibitors for mild steel in acidic medium: Electrochemical, SEM, AFM, and XPS studies, *J. Mol. Liq.*, 2016, **216**, 164–173, DOI: 10.1016/j.molliq.2015.12.086.

75 Y. Qiang, *et al.*, Sodium dodecyl benzene sulfonate as a sustainable inhibitor for zinc corrosion in 26% NH4Cl solution, *J. Clean. Prod.*, 2017, **152**, 17–25, DOI: 10.1016/j.jclepro.2017.03.104.

76 Y. El Kacimi, *et al.*, Anti-corrosion Properties of 2-Phenyl-4(3H)-quinazolinone-Substituted Compounds: Electrochemical, Quantum Chemical, Monte Carlo, and Molecular Dynamic Simulation Investigation, *J. Bio- Tribo-Corrosion*, 2020, **6**(2), 1–25, DOI: 10.1007/s40735-020-00342-1.

77 G. Gece, The use of quantum chemical methods in corrosion inhibitor studies, *Corros. Sci.*, 2008, **50**(11), 2981–2992, DOI: 10.1016/j.corsci.2008.08.043.

78 H. Ju, L. Ding, C. Sun and J. J. Chen, Quantum Chemical Study on the Corrosion Inhibition of Some Oxadiazoles, *Adv. Mater. Sci. Eng.*, 2015, **2015**, 1–5, DOI: 10.1155/2015/519606.

79 Y. Boughoues, M. Benamira, L. Messaadia, N. Bouider and S. Abdelaziz, Experimental and theoretical investigations of four amine derivatives as effective corrosion inhibitors for mild steel in HCl medium, *RSC Adv.*, 2020, **10**(40), 24145–24158, DOI: 10.1039/d0ra03560b.

80 B. A. Abd-El-Nabey, M. E. Mohamed, A. M. Helmy, H. Elnagar and A. M. Abdel-Gaber, Eco-friendly corrosion inhibition of steel in acid pickling using Prunus domestica Seeds and Okra stems extracts, *Int. J. Electrochem. Sci.*, 2024, **19**(8), 100695, DOI: 10.1016/j.ijoes.2024.100695.

81 A. Martínez, E. Perez-Sanchez, A. Caballero, R. Ramírez, E. Quevedo and D. Salvador-García, PBAT is biodegradable but what about the toxicity of its biodegradation products?, *J. Mol. Model.*, 2024, **30**(8), 1–7, DOI: 10.1007/s00894-024-06066-0.

82 M. Dehdab, M. Shahraki and S. M. Habibi-Khorassani, Theoretical study of inhibition efficiencies of some amino acids on corrosion of carbon steel in acidic media: Green corrosion inhibitors, *Amino Acids*, 2016, **48**(1), 291–306, DOI: 10.1007/s00726-015-2090-2.

83 M. Shahraki, M. Dehdab and S. Elmi, Theoretical studies on the corrosion inhibition performance of three amine derivatives on carbon steel: Molecular dynamics simulation and density functional theory approaches, *J. Taiwan Inst. Chem. Eng.*, 2016, **62**, 313–321, DOI: 10.1016/j.jtice.2016.02.010.

84 O. E. Oyeneyin, N. D. Ojo, N. Ipinloju, A. C. James and E. B. Agbaffa, Investigation of Corrosion Inhibition Potentials of Some Aminopyridine Schiff Bases Using Density Functional Theory and Monte Carlo Simulation, *Chem. Africa*, 2022, **5**(2), 319–332, DOI: 10.1007/s42250-021-00304-1.

85 N. Raghavendra and J. Ishwara Bhat, Benevolent Behavior of Arecanut Husk Extracts as Potential Corrosion Inhibitor for Aluminum in both 0.5 M HCl and 0.1 M NaOH Environments, *J. Bio- Tribo-Corrosion*, 2018, **4**(3), 1, DOI: 10.1007/s40735-018-0159-7.

86 R. Padash, A. H. Jafari and E. Jamalizadeh, Experimental and theoretical study of aluminium corrosion in NaOH, NaCl and HCl solutions, *Anti-Corrosion Methods Mater.*, 2018, **65**(4), 350–360, DOI: 10.1108/ACMM-04-2017-1785.

87 A. S. Fouda, S. M. Abd El-Wahab, M. S. Attia, A. O. Youssef and H. O. Elmoher, Chemical and electrochemical studies of para-Hydroazo-pyrazolone derivatives as corrosion inhibitors for mild steel in hydrochloric acid solutions, *Int. J. Electrochem. Sci.*, 2015, **10**(9), 7866–7892, DOI: 10.1016/s1452-3981(23)17396-2.

88 N. S. Abdelshafi, M. A. Sadik, M. A. Shoeib and S. A. Halim, Corrosion inhibition of aluminum in 1 M HCl by novel pyrimidine derivatives, EFM measurements, DFT calculations and MD simulation, *Arab. J. Chem.*, 2022, **15**(1), 103459, DOI: 10.1016/j.arabjc.2021.103459.

89 O. S. Amodu, M. O. Odunlami, J. T. Akintola, T. V. Ojumu and O. S. Ayanda, Artificial neural network and response surface methodology for optimization of corrosion inhibition of mild steel in 1 M HCl by Musa paradisiaca peel extract, *Heliyon*, 2022, **8**(12), e11955, DOI: 10.1016/j.heliyon.2022.e11955.

90 O. Meena, S. Kaushal, S. Kumar and J. Dalal, Euphorbia neriifolia extracts as green corrosion inhibitors for aluminium in hydrochloric and nitric acid media, *Discov. Mater.*, 2024, **4**(1), 102–126, DOI: 10.1007/s43939-024-00157-8.

91 O. O. Onukwuli, B. C. Udeh, M. Omotioma and I. A. Nnanwube, Corrosion inhibition of aluminium in hydrochloric acid medium using cimetidine as inhibitor: empirical and optimization studies, *Anti-Corrosion Methods Mater.*, 2021, **68**(5), 385–395, DOI: 10.1108/ACMM-03-2021-2447.

92 K. Bouiti, *et al.*, Response surface methodology for optimizing corrosion inhibition: investigating the synergistic effect of Eriobotrya japonica extract and potassium iodide, *Euro-Mediterranean J. Environ. Integr.*, 2024, **9**(2), 469–481, DOI: 10.1007/S41207-023-00457-0.